Turkish Journal of Chemistry

Volume 42 | Number 2 Article 11

1-1-2018

The synthesis of new oxindoles as analogs of natural product 3,3$^\prime $-bis(indolyl)oxindole and in vitro evaluation of the enzyme activity of G6PD and 6PGD

SİNAN BAYINDIR

ADNAN AYNA

YUSUF TEMEL

MEHMET ÇİFTCİ

Follow this and additional works at: https://journals.tubitak.gov.tr/chem

Part of the Chemistry Commons

Recommended Citation

BAYINDIR, SİNAN; AYNA, ADNAN; TEMEL, YUSUF; and ÇİFTCİ, MEHMET (2018) "The synthesis of new oxindoles as analogs of natural product 3,3$^\prime $-bis(indolyl)oxindole and in vitro evaluation of the enzyme activity of G6PD and 6PGD," *Turkish Journal of Chemistry*: Vol. 42: No. 2, Article 11.
https://doi.org/10.3906/kim-1706-51
Available at: https://journals.tubitak.gov.tr/chem/vol42/iss2/11

This Article is brought to you for free and open access by TÜBİTAK Academic Journals. It has been accepted for inclusion in Turkish Journal of Chemistry by an authorized editor of TÜBİTAK Academic Journals. For more information, please contact academic.publications@tubitak.gov.tr.

Turkish Journal of Chemistry

http://journals.tubitak.gov.tr/chem/

Research Article

Turk J Chem
(2018) 42: 332 – 345
© TÜBİTAK
doi:10.3906/kim-1706-51

The synthesis of new oxindoles as analogs of natural product 3,3′-bis(indolyl)oxindole and in vitro evaluation of the enzyme activity of G6PD and 6PGD

Sinan BAYINDIR[1,*], **Adnan AYNA**[1], **Yusuf TEMEL**[2], **Mehmet ÇİFTCİ**[1]
[1]Department of Chemistry, Faculty of Sciences and Arts, Bingöl University, Bingöl, Turkey
[2]Department of Health Services, Vocational Schools, Bingöl University, Bingöl, Turkey

Received: 22.06.2017 • **Accepted/Published Online:** 30.10.2017 • **Final Version:** 27.04.2018

Abstract: Natural and synthetic derivatives that contain an indole core are being used in medical treatments and technological processes. Therefore, the development of new synthetic methods for the synthesis of indole derivatives is very popular. In this study, new oxindoles with reaction of 4,7-dihydro-1*H*-indole (**2**) and isatin (**4**) were synthesized as analogs of natural product 3,3′-bis(indolyl)oxindole. The biological properties of the compounds obtained during this study were also studied, showing that compounds **5**, **7**, and **12** inhibited the activity of G6PD with an IC_{50} of 99 μM, 231 μM, and 304 μM respectively. The activity of rat erythrocyte 6PGD was increased in the presence of **5** and **7** and was inhibited in the presence of **12**. As indole derivative **5** was an activator of 6PGD and inhibitor of G6PD, it was selected for docking studies to understand the mechanism of activation and inhibition.

Key words: Oxindoles, natural product, 3,3′-bis(indolyl)oxindole, enzyme, 6PGD, G6PD

1. Introduction

Natural compounds with more than one indole skeleton have been reported to show anticancer activity by interacting with different cellular targets.[1−8] The 3,3′-bisindole oxindole and 3-substituted oxindole skeleton belongs to a class of privileged heterocyclic frameworks, which constitutes the core structures of many bioactive compounds (Figure 1). Additionally, 2-alkylindoles and 2.2′-bis(indolyl)methanes represent quite an interesting class and are also known to play an important role in numerous biological and technological processes.[9−12] Therefore, a great deal of attention has been given to the development of effective, facile, and innovative synthetic strategies for the enhancement of indole chemistry. Indole is an electron-rich heteroaromatic system, and although various methods for synthesis of C3-substituted derivatives are well known, the synthesis of C2-substituted derivatives continues to be a difficult task.[13−24] While a number of methods have already been published for the synthesis of 3-substituted indole derivatives, there are no methods for the synthesis of 2-substituted indole derivatives through the indole ring. An alternative method that utilizes 4,7-dihydro-1*H*-indole (**2**) derivatives as synthetic equivalents (synthons) for easy synthesis of 2-substituted indoles was developed by Saraçoğlu and coworkers[25−28] (Figure 2). The indole (**1**) exhibits reactivity at the C-3 position against the electrophiles and forms the 3-substituent indole derivatives at the end of the reaction. The advantage of this strategy developed by Saraçoğlu and coworkers is that the derivatives **2** and **3** obtained as a result of

*Correspondence: snanbay@atauni.edu.tr

reduction of the indole (**1**) are also pyrrole derivatives. The obtained molecules **2** and **3** electrophilically react with C-2 carbon to give 2-substituted indole derivatives (Figure 2).

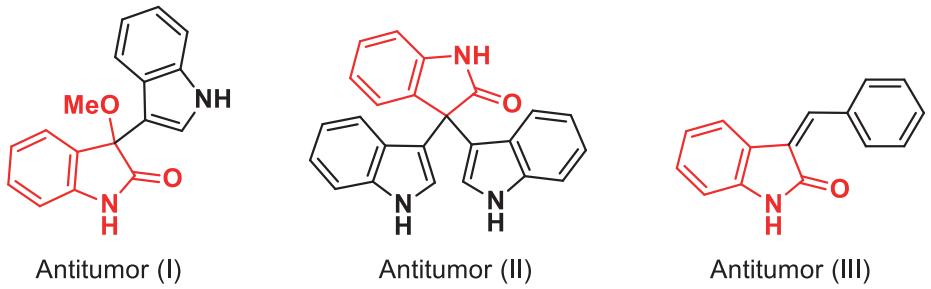

Figure 1. Chemical structures of compounds containing 3,3′-bisindole and indolin-2-one framework.

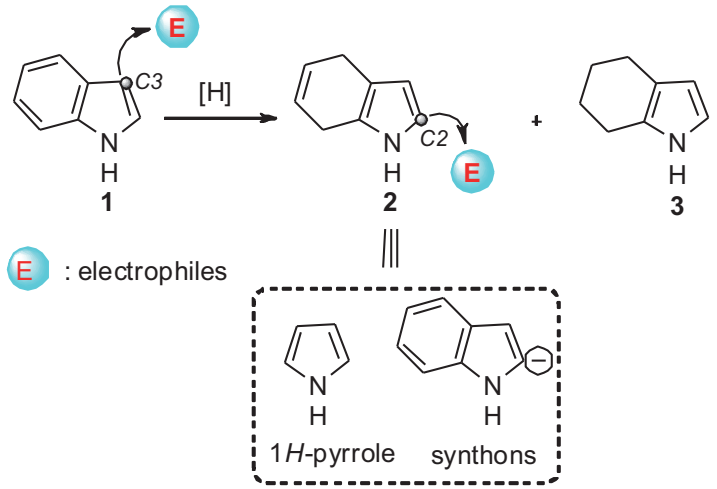

Figure 2. Reactivity of indole (**1**) and 4,7-dihydro-1*H*-indole (**2**).

The technological applications of synthetic indole derivatives have attracted a great deal of interest in recent years.[29−31] In this context, the indole skeleton is a highly used unit for biological chemosensor applications. Previous studies of bisindole derivatives revealed that they alter the enzymatic activity of some enzymes like human carbonic anhydrase isoforms I-II and α/β-glycosidase. In a recent study, the antioxidant activities of 1,4-bis(indolin-1-ylmethyl)benzene derivatives were reported by Talaz and coworkers.[32] However, there is no study investigating the effect of such compounds on metabolic enzymes including glucose-6-phosphate dehydrogenase (G6PD; E.C.1.1.1.49) and 6-phosphogluconate dehydrogenase (6PGD; E.C.1.1.1.44). Therefore, one aim of the work described in this paper is to investigate the effect of indole derivatives on the activity of the corresponding enzymes. G6PD is the rate-limiting enzyme of the pentose phosphate pathway. It catalyzes the irreversible conversion of glucose 6-phosphate to 6-phosphoglucono-δ-lactone in the presence of $NADP^+$.[33] 6PGD is the third enzyme in the pentose phosphate pathway. It is a well-known oxidative carboxylase that catalyzes conversion of 6-phosphogluconate into ribulose 5-phosphate.[34] The pentose phosphate pathway is one of the key components of cellular metabolism. It is strongly connected to glycolysis as a major consumer of glucose. The primary roles of the pathway are generating NADPH as a source of reducing power and the synthesis of ribose 5-phosphate, which is required for the synthesis of nucleic acids.[35,36] In the absence of these

enzymes the erythrocyte is susceptible to oxidative damage. G6PD is also associated with some human diseases including cancer, metabolic disorders, and cardiovascular diseases.[37–39] It was also reported that suppression of 6PGD decreased lipogenesis and RNA biosynthesis and increased reactive oxygen levels in cancer cells, lessening cell proliferation and tumor growth and suggesting that 6PGD could be an anticancer target.[40]

In our previous studies, we developed an efficient, facile, and atom-economical protocol for the preparation of 2-alkylated indoles and bis(2-indolyl)methanes derivatives through addition of one or two equivalents of 4,7-dihydro-1*H*-indole (**2**) using ketones as electrophiles followed by an oxidation step[28] (Scheme 1a). Herein, $Bi(NO_3)_3 5H_2O$-catalyzed reactions of 4,7-dihydro-1*H*-indole (**2**) with isatin (**4**) (Scheme 1b) and the obtained molecules were examined along with investigating their effects on the enzymatic activity of rat erythrocyte G6PD and 6PGD and docking studies.

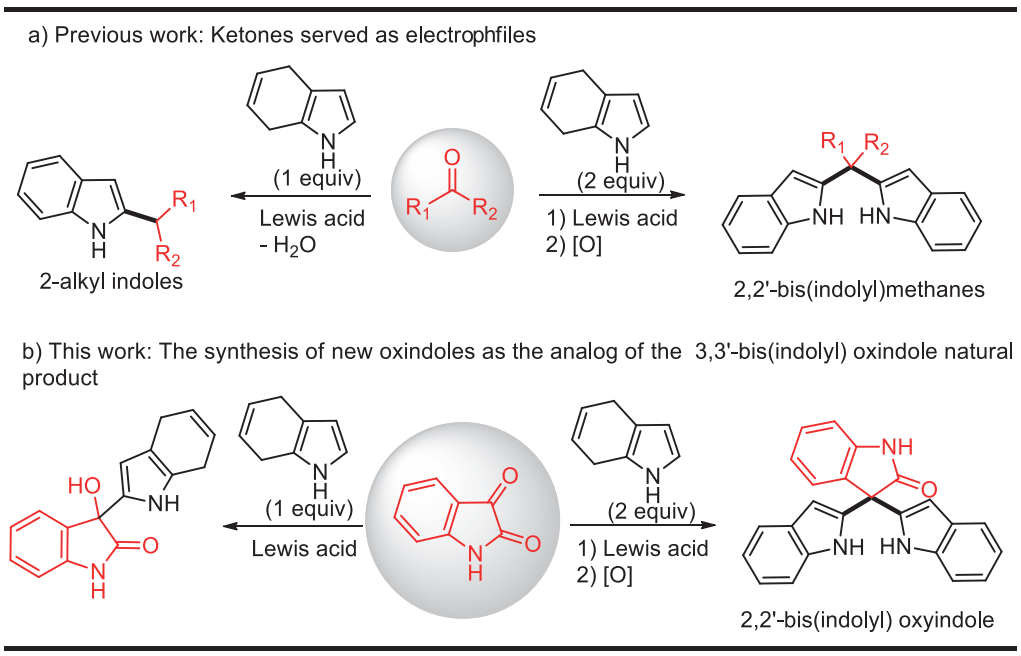

Scheme 1. Strategies for the reactions of 4,7-dihydro-1*H*-indole (**2**) with isatin (**4**).

2. Results and discussion

2.1. Chemistry

Our research interest in the synthesis of new oxindole derivatives with 1,2- and 1,3-diketones of 4,7-dihydro-1*H*-indole (**2**) encouraged us to ascertain the behavior of ketones having a different nature against the condensation reactions of 4,7-dihydro-1*H*-indole (**2**). In this context, initially 4,7-dihydro-1*H*-indole, which was used as an output molecule in the reactions, was synthesized via Birch reduction reaction of indole with Li in liquid ammonia. The Birch reduction, a very powerful reducing system, has been reported to yield a mixture of 4,7-dihydro-1*H*-indole (**2**) and 4,5,6,7-tetrahydroindole (**3**) in a 4:1 ratio according to NMR, which could be best separated by recrystallization or distillation.[25–28] Isatin (**4**) as an 1,2-diketone derivative has provided an opportunity to investigate the effect of the carbonyl group on the condensation of 4,7-dihydro-1*H*-indole (**2**) with ketone (Scheme 2). As shown in Table 1, the reaction of 4,7-dihydro-1*H*-indole with isatin (**4**) was

first assayed with the $Bi(NO_3)_3 5H_2O$ catalyst at room temperature. However, no product formation was observed under these conditions (Table 1, entry 5). The bismuth nitrate-catalyzed reaction of 4,7-dihydro-1*H*-indole with isatin (**4**) in CH_3CN at reflux temperature gave alcohol derivative 3-(4,7-dihydro-1*H*-indol-2-yl)-3-hydroxyindolin-2-one (**5**) in 98% yield instead of the expected product **6** (Table 1, entry 6). Additionally, a very complex mixture with trifluoroacetic acid (TFA), $ZrCl_4$, $AlCl_3$, and PhCOOH catalysts was obtained at room temperature (Table 1, entries 1–4). As a result of the reaction, the synthesis of indole derivative **6** was expected by elimination of 1 mol of water and 1 mol of protons from alcohol derivative **5**. However, it was observed that the intermediate product, alcohol derivative **5**, was more stable, and it was obtained as the main product (Scheme 2). It was seen that NH groups resonated at 10.4 and 10.2 ppm in the ^{1}H NMR spectrum of unexpected bisindole derivative **5**. One proton available in the alcohol units resonated at 5.26 ppm. All these signals support the recommended structure.

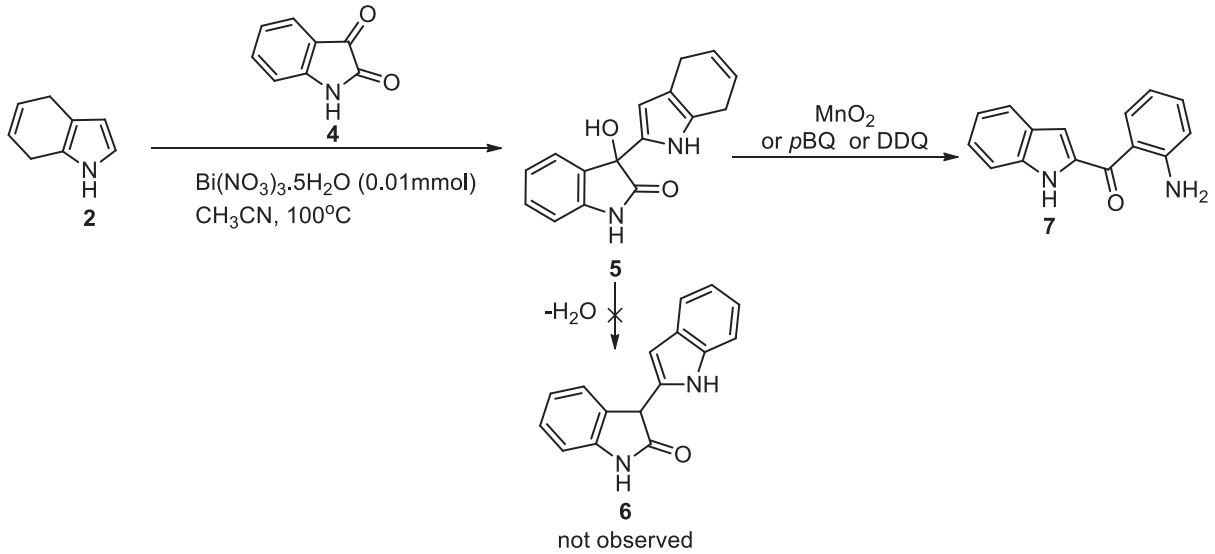

Scheme 2. The synthesis of **5** and **7**.

Surprisingly, the oxidation of alcohol derivative **5** with MnO_2 produced unexpected amine derivative (2-aminophenyl)(1*H*-indol-2-yl)methanone (**7**) in 81% yield instead of the expected product **8** (Schemes 2 and 3). The same results were obtained with *p*-benzoquinone (*p*BQ) or DDQ (2,3-dichloro-5,6-dicyano-1,4-benzoquinone) in 25% and 12% yields, respectively. It was seen that one NH group resonated at 9.29 ppm in the ^{1}H NMR spectrum of unexpected amine derivative **7**. The two protons available in amine units resonated at 5.71 ppm. Also, while the ^{13}C NMR resonance signal was available at 177.0 ppm in the ^{13}C NMR spectrum of unexpected amine derivative **7**, the signal shows the existence of a ketone group in the molecule and 14 carbon resonance signals in the aromatic area, supporting the recommended structure (Scheme 2). Because of the sensitivity of the carbonyl group toward moisture the hydration of the carbonyl group undergoes carbon/nitrogen bond cleavage to give unexpected amine derivative **7** and carbon dioxide (Scheme 3).

Bis/tris-indole derivatives are an important class of biological active indoles. In this context, the reaction of 2 equivalents of 4,7-dihydro-1*H*-indole (**2**) with one equivalent of isatin (**4**) was also performed under similar conditions (Scheme 4). The 2,2′-bis(indolyl)oxindole (**12**), which resembles anticancer agent 3,3′-bis(indolyl)oxindole, was synthesized by condensation of 4,7-dihydro-1*H*-indole (**2**, 2 equiv.) with isatin (**4,** 1

Table 1. Optimization of reaction conditions.[a]

Entry	Catalyst	Solvent	Temp. (°C)	Time	Yield[b] (%)
1	TFA	CH_2Cl_2	RT	30 min.	0[c,d]
2	$AlCl_3$	CH_2Cl_2	RT	30 min.	0[c,d]
3	PhCOOH	CH_2Cl_2	RT	30 min.	0[c,d]
4	$ZrCl_4$	CH_2Cl_2	RT	30 min.	0[c,d]
5	$Bi(NO_3)_3 5H_2O$	CH_2Cl_2	RT	12h	0
6	$Bi(NO_3)_3 5H_2O$	MeCN	Reflux	5h	98
7	$Cu(OTf)_2$	MeCN	Reflux	5h	56[c,d]
8	$InCl_3$	MeCN	Reflux	5h	11[c,d]
9	$Zn(OTf)_2$	MeCN	Reflux	5h	61[c,d]
10	$BiCl_3$	MeCN	Reflux	5h	72

[a]:Conditions: 4,7-dihydro-1*H*-indole (**2**, 1 equiv.), isatin (**4**, 1 equiv.), catalyst (0.1 mmol), and solvent (10 mL). [b]:Isolated yields of **5**. [c]:Complex reaction mixture. [d]:Under N_2.

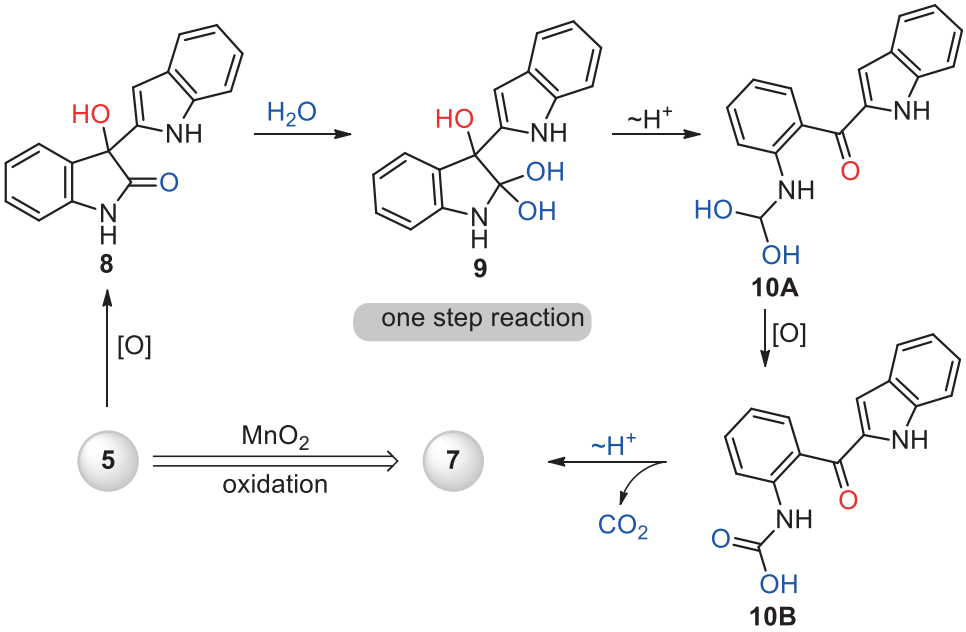

Scheme 3. Proposed mechanism for synthesis of unexpected

equiv.) catalyzed by $Bi(NO_3)_3 5H_2O$ in CH_3CN, followed by an oxidation reaction by *p*-benzoquinone over 4,7-dihydro-1*H*-indole derivative **11** (Scheme 4). Despite all attempts, 4,7-dihydro-1H-indole derivative **11**, which was seen from NMR spectra, could not be isolated.

Additionally, the reactions of 4,7-dihydro-1*H*-indole (**2**) with other 1,2- and 1,3-diketones such as 2,3-butanedione (**13**), acenaphthoquinone (**14**), and cyclohexane-1,3-dione (**15**) were examined under the same conditions (Figure 3). No significant results were obtained from the studies of 1,2-diketones. While the reaction of diketones **13** and **14** gave no isolable product, no reaction was observed with cyclohexane-1,3-dione (**15**).

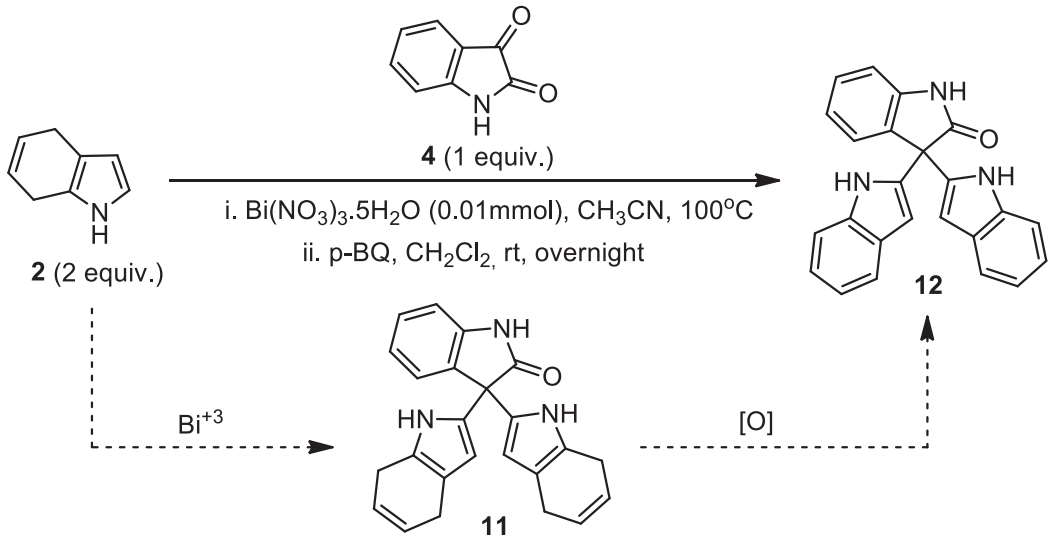

Scheme 4. The synthesis of **12**.

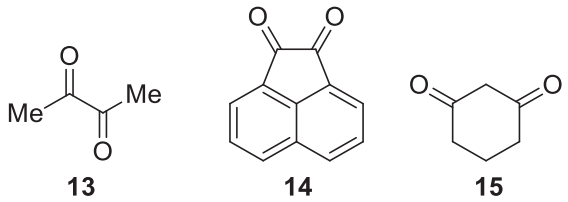

Figure 3. The chemical structures of other 1,2- and 1,3-diketones examined.

2.2. G6PD and 6PGD inhibition/activations studies

Following synthesis of the bisindole derivatives **5**, **7**, and **12**, investigation of the effects of these derivatives on rat blood erythrocyte G6PD and 6PGD was conducted. In order to achieve that, first G6PD and 6PGD were purified from rat blood erythrocytes by 2′,5′-ADP Sepharose 4B affinity chromatography.[41−43] Following purification, the in vitro effects of ligands **5**, **7**, and **12** on the activity of both enzymes were investigated. The inhibition effect of the compounds on enzymes is expressed in IC_{50} values and K_i constants. Derivatives **5**, **7**, and **12** inhibited the activity of G6PD with an IC_{50} of 99 μM, 231 μM, and 304 μM, respectively (Table 2, Figure S8, ESI). To further understand the mechanism by which these compounds inhibited these enzymes, the inhibitory modes of the derivatives were studied. The collected raw data were described as Lineweaver–Burk diagrams and suggested that all derivatives except **5** inhibited the activity of G6PD noncompetitively with respect to G6P as the reaction rate was decreased and K_m remained unchanged while **5** was a competitive inhibitor of G6PD. Their K_i values were calculated based on this diagram to be 48 μM, 369 μM, and 304 μM respectively (Figure S9, ESI). As suggested by the IC_{50} and K_i values of each compound, inhibition is most powerful by ligand **5**. This could be attributed to the hydrogen bonding capacity of the compounds with the amino acid residues of the enzyme. Indole derivative **5** has three groups that can make hydrogen bonds and it also has oxygen, which is more electronegative than other atoms, which makes it form stronger hydrogen bonds with the amine group of the amino acid residues. These properties may make indole derivative **5** a more powerful inhibitor than the others.

Table 2. Determination of IC_{50} and K_i values and inhibition types of the compounds.

G6PD			
Ligand	IC_{50} (μM)	Ki (μM)	Type of inhibition
5	99	48	Competitive
7	231	369	Noncompetitive
12	304	304	Noncompetitive
6PGD			
Ligand	IC_{50} (μM)	Ki (μM)	Type of inhibition
5	N/A	N/A	N/A
7	N/A	N/A	N/A
12	209	N/A	N/A

The effects of these compounds on 6PGD were also tested. Unlike G6PD, the activity of 6PGD was increased approximately fourfold (380%) in the presence of 250 μM indole derivative **5** and the activity was increased approximately twofold (176%) in the presence of 1500 μM indole derivative **7**. However, activity was inhibited in the presence of indole derivative **12** with an IC_{50} of 209 μM (Table 2, Figure S10, ESI).

2.3. Molecular docking analysis

The inhibition studies revealed that compound **5** inhibited the activity of G6PD competitively. To elucidate the binding modes of **5** in rat erythrocyte G6PD, a homology model of the structure of the enzyme was generated and ligand **5** was docked. Docking experiments gave approximately 250 poses. Careful examination of each pose revealed that the ligand is located in the $NADP^+$ binding domain and fits in the position of $NADP^+$, making weak interactions with the residues around the binding site (Figures 4a–4c and S12, ESI). This result supports experimental studies demonstrating that the enzyme is competitively inhibited by ligand **5**. The oxygen atom of the ketone group in **5** makes a hydrogen bond (4 Å) with the NH group of Gly41. Similarly, the OH group of **5** will form a hydrogen bond (3.4 Å) with the N atom of Asp42. While the C_4-H (acidic proton) of the 4,7-dihydro indole unit makes a hydrogen bond (2.9 Å) with the NH group of Pro143, the C_7-H (acidic proton) atom of the 4,7-dihydro indole unit forms a hydrogen bond (3.9 Å) with the NH group of the pyrrole ring in Pro143 (Figure 4b). $NADP^+$ makes similar interactions with the residues around it. The inhibition of the enzyme might be caused by the replacement of $NADP^+$ by **5**.

In contrast to its effect on G6PD, the presence of the ligand increased the activity of 6PGD. To further understand the effect, the structure of the enzyme was generated by homology modeling and docking studies were performed. The results of docking studies were analyzed manually (Figures 5a–5d and S11, ESI). It was revealed that the ligand was located close to the substrate and ligand binding site without interacting with any residues around it. It was postulated that the ligand could assist in increasing the activity of the enzyme by reducing $NADP^+$ to NADPH. In catalysis, two residues, one acting as an acid (Glu) and the other as a base (Lys), are proposed to contribute to all three catalytic steps of the reaction catalyzed by 6PGD: dehydrogenation, decarboxylation, and keto-enol tautomerization. Lys is thought to be unprotonated in the enzyme/substrate complex, where it takes a proton from the 3-OH of 6PGA as a hydride that is transferred from the C3 of 6PGA to $NADP^+$. The resultant 3-keto-6PGA intermediate is subsequently decarboxylated to

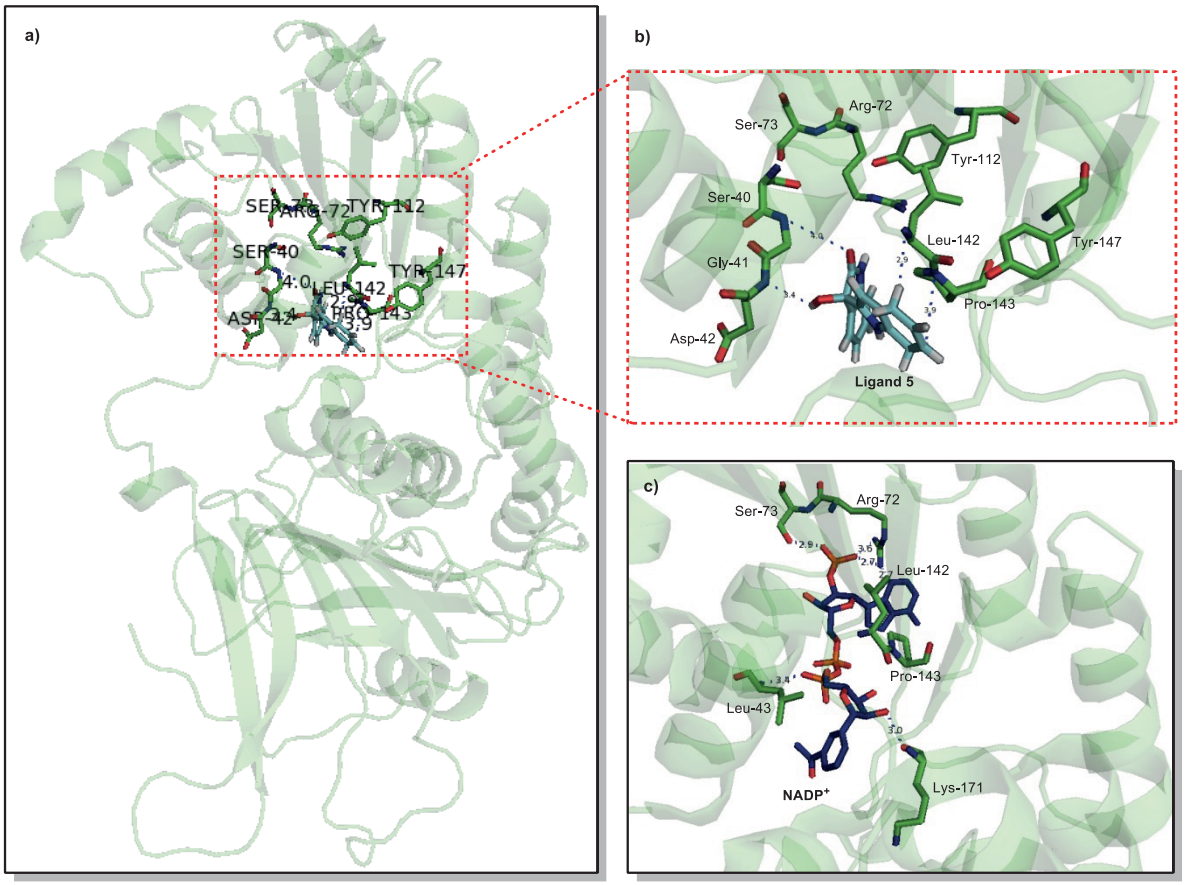

Figure 4. a) Representation of the binding site of ligand **5**, b) zoomed view of binding site of ligand **5**, and c) NADP$^+$ binding site of G6PD.

form the enediol of 5-phospho-ribulose. At this stage, Glu donates a proton to the C_3 carbonyl group of the keto intermediate to facilitate decarboxylation. Both a base and an acid are essential in the tautomerization of the enediol intermediate to form ribulose 5-phosphate, with Glu giving a proton to the C1 of the enediol intermediate and the base accepting a proton from its 2-OH.[44–47]

As shown in Figures 5a–5d and Scheme 5, it is proposed that NADP$^+$ will assist in converting 6PGA to R5P. Following that, it will oxidize the 4,7-dihydro indole unit in ligand **5** to an indole unit. The amino group of an arginine residue located in the close vicinity of **5** will behave as a base and attack the C_7-H of 4,7-dihydro-1H-indole, forming an aromatic ring, which is then receiving protons from C_4-H and reduces NADP$^+$ to NADPH, thus increasing the activity of the enzyme (Scheme 5).

In conclusion, we have reported the synthesis of possible biologically active new indoles 3-(4,7-dihydro-1H-indol-2-yl)-3-hydroxyindolin-2-one (**5**), (2-aminophenyl)(1H-indol-2-yl)methanone (**7**), and 1H,1$''H$-[2,3$'$:3$'$,2$''$-terindol]-2$'$(1$'H$)-one (**12**) from the reaction of 4,7-dihydro-1H-indole (**2**) with isatin (**4**) and have discussed the formation mechanism. In addition to synthesis, effects of indole derivatives **5**, **7**, and **12** on the activity of erythrocyte G6PD and 6PGD have also been investigated in in vitro conditions. These studies showed that **5**, **7**, and **12** inhibited the activity of G6PD with an IC50 of 99 μM, 231 μM, and 304 μM, respectively. However, studies on rat erythrocyte 6PGD indicated that the activity was increased in the presence of **5** and

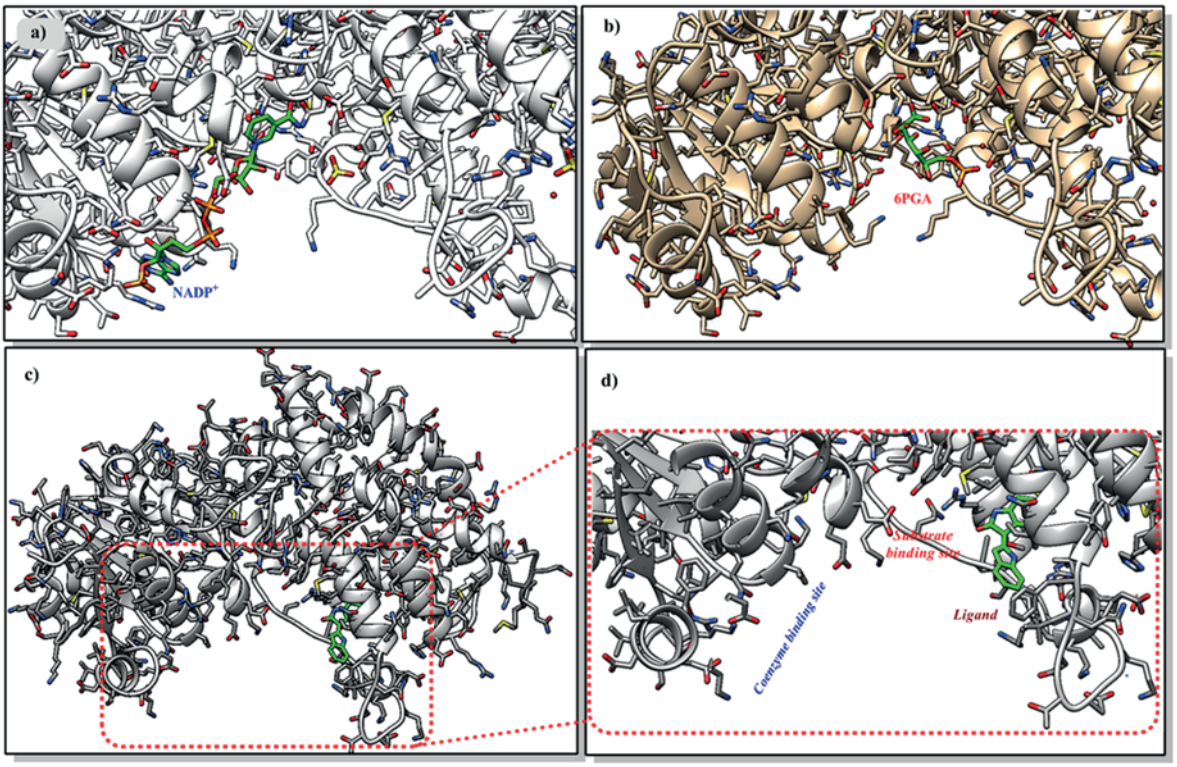

Figure 5. a) Representation of NADP$^+$ (PDB-ID: 1PGN), b) 6PGA (PDB-ID: 1PGP), c) binding site of **5**, and d) zoomed view of binding sites in 6PGD. The binding sites of NADP$^+$ and 6PGA were derived from crystal structures and the binding site for **5** was calculated via docking.

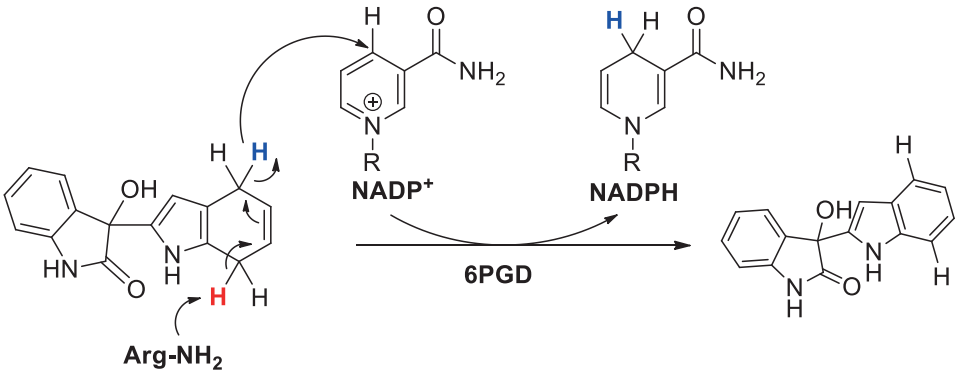

Scheme 5. Proposed mechanism for oxidation of **5** with 6PGD.

7 and was inhibited in the presence of **12**. As ligand **5** inhibited one enzyme and activated the other, it was selected for docking experiments. The analyses of docking results suggested that the ligand binds the NADP$^+$ binding site in G6PD while it is located in the close vicinity of the substrate and NADP$^+$ binding sites donating a hydride to NADP, hence increasing the activity of 6PGD.

3. Experimental

All chemicals, reagents, and solvents were commercially available from Sigma-Aldrich or Merck and were used as received. 2′,5′-ADP Sepharose 4B was purchased from Pharmacia. Melting points were determined on a

Buchi 539 capillary melting apparatus and are uncorrected. Infrared spectra were recorded on a Mattson 1000 FT-IR spectrophotometer. ^{1}H NMR and ^{13}C NMR spectra were recorded on a 400 (100)-MHz Varian and Bruker spectrometer and are reported in terms of chemical shift (δ, ppm) with $SiMe_4$ as an internal standard. Data for ^{1}H NMR are recorded as follows: chemical shift (δ, ppm), multiplicity (s: singlet, d: doublet, t: triplet, q: quartet, p: pentet, m: multiplet, bs: broad singlet, bd: broad doublet, qd: quasi doublet) and coupling constant (s) in Hz, integration. Elemental analyses were carried out on a LECO CHNS-932 instrument. Column chromatography was carried out on silica gel 60 (230–400 mesh ASTM). The reaction progress was monitored by thin-layer chromatography (TLC) (0.25-mm-thick precoated silica plates: Merck Fertigplatten Kieselgel (60 F254)). UV-Vis spectra were recorded on a Shimadzu UV-3101PL UV-Vis-NIR spectrometer.

3.1. Synthesis of 4,7-dihydro-1H-indole (2)

Compound **2** was prepared according to the literature method.[25,28] Liquid ammonia (500 mL) was distilled under N_2 into a predried three-necked flask. Then the solution of indole (**1**, 25 g, 0.21 mol) in dry Et_2O (100 mL) was added and the resulting solution was cooled to –35 °C and stirred mechanically. The resulting solution was treated with lithium metal (6 g, 0.84 mol) added in small pieces for 5–10 min, which reacted very rapidly. The resulting deep blue solution was stirred at the same temperature for 1 h and then the mixture was transferred to room temperature. After the excess ammonia had evaporated, Et_2O (200 mL), NH_4Cl (5 g), and H_2O (300 mL) were carefully added to the reaction mixture. The layers were separated, the aqueous layer was extracted with Et_2O (2 × 200 mL), and the combined organic layers were washed with $NaHCO_3$ (2 × 100 mL), dried ($MgSO_4$), filtered, and concentrated. The ^{1}H NMR spectrum of the residue showed the formation of 4,7-dihydro-1*H*-indole (**2**) and 4,5,6,7-tetrahydro-1*H*-indole (**3**) in a 4:1 ratio. The crude product (23 g) was recrystallized with hexane to give 4,7-dihydro-1*H*-indole (**2**) (white solid, mp: 38–39 °C, 19 g, 75%) as colorless crystals.

^{1}H NMR (400 MHz, $CDCl_3$): δ 7.70 (m, NH, 1H), 6.72 (t, J = 2.5 Hz, =CH, 1H), 6.07 (t, J = 2.5 Hz, =CH, 1H), 5.95 (bd, J = 10.1 Hz, =CH, 1H), 5.87 (bd, J = 10.1 Hz, =CH, 1H), 3.30 (bs, CH_2, 4H); ^{13}C NMR (100 MHz, $CDCl_3$): δ 128.0, 127.9, 125.98, 118.3, 115.9, 108.8, 27.1, 26.0.

3.2. The reaction of 4,7-dihydro-1*H*-indole (2, 1 equiv.) with isatin (4, 1 equiv.)

To a solution of 4,7-dihydro-1*H*-indole (**2**, 200 mg, 1.68 mmol) in MeCN (5 mL), indoline-2,3-dione (**4**, isatin, 247 mg, 1.68 mmol) and $Bi(NO_3)_3 \cdot 5H_2O$ (0.1 mmol) were added. The reaction mixture was stirred magnetically in a flask at 100 °C. The reaction was monitored by TLC. After the completion of the reaction, the mixture was diluted with ethyl acetate (30 mL) and washed with water (2 × 50 mL), and the organic phase was dried over Na_2SO_4. The crude product was purified by silica gel column chromatography and the isolated compound was given according to the elution sequence (EtOAc/Hexane; v/v: 1/3). After purification, 3-(4,7-dihydro-1*H*-indol-2-yl)-3-hydroxyindolin-2-one (**5,** 437 mg, 98%) was obtained as a pale yellow solid (mp: 165–166 °C (crystallized over CH_2Cl_2/hexane)).

^{1}H NMR (400 MHz, DMSO-d6): δ 10.42 (bs, NH, 1H), 10.21 (s, NH, 1H), 7.38 (d, J = 7.6 Hz, =CH, 1H), 7.20 (t, J = 7.6 Hz, =CH, 1H), 6.97 (t, J = 7.6 Hz, =CH, 1H), 6.79 (d, J = 7.6 Hz, =CH, 1H), 7.31 (s, =CH, 1H), 5.77 (m, =CH, 2H), 5.27 (qd, J = 2.5 Hz, OH, 1H), 3.30–3.27 (m, CH_2, 2H), 3.17–3.13 (m, CH_2, 2H); ^{13}C NMR (100 MHz, DMSO-d6): δ 178.3, 142.2, 133.1, 129.6, 129.4, 126.0, 125.7, 125.6, 124.2, 122.2,

112.3, 110.2, 105.5, 74.1, 25.1, 24.6; IR (KBr, cm^{-1}): 3426, 3403, 3342, 3036, 2918, 2876, 2851, 2725, 2685, 1714, 1605, 1469, 1208, 870, 740; Anal. Calcd. for $C_{16}H_{14}N_2O_2$: C, 72.17; H, 5.30; N, 10.52; found: C, 72.57; H, 5.31; N, 10.97; TLC: R_f = 0.12 (EtOAc/hexane (v/v: 1/3), 254 nm).

3.3. The oxidation of 3-(4,7-dihydro-1*H*-indol-2-yl)-3-hydroxy indolin-2-one (5)

Procedure A: To a solution of 3-(4,7-dihydro-1*H*-indol-2-yl)-3-hydroxyindolin-2-one (**5**, 300 mg, 1.13 mmol) in 10 mL of CH_2Cl_2 was added MnO_2 (980 mg, 11.3 mmol). After stirring for 12 h at room temperature, the mixture was diluted with EtOAc (30 mL) and washed with water (3 × 30 mL), and the organic phase was dried over Na_2SO_4. The crude product (230 mg) was eluted on silica gel (25 g) with EtOAc/hexane (v/v: 3/7). After purification, (2-aminophenyl)(1*H*-indol-2-yl)methanone (**7**, 215 mg, 81%) was obtained as a white solid (mp: 115–116 °C (crystallized over CH_2Cl_2/ hexane)).

Procedure B: (2-Aminophenyl)(1*H*-indol-2-yl)methanone (**7**) was obtained as a white solid (67 mg, 25%) from the reaction of 3-(4,7-dihydro-1*H*-indol-2-yl)-3-hydroxyindolin-2-one (**5,** 300 mg, 1.13 mmol) with *p*-benzoquinone (304 mg, 2.82 mmol) in CH_2Cl_2 at room temperature for 12 h.

Procedure C: (2-Aminophenyl)(1H-indol-2-yl)methanone (**7**) was obtained as a white solid (32 mg, 12%) from the reaction of 3-(4,7-dihydro-1*H*-indol-2-yl)-3-hydroxyindolin-2-one (**5,** 300 mg, 1.13 mmol) with DDQ (640 mg, 2.82 mmol) in CH_2Cl_2 at room temperature for 12 h.

^{1}H NMR (400 MHz, $CDCl_3$): δ 9.29 (bs, NH, 1H), 8.01 (d, J = 8.1 Hz, =CH, 1H), 7.71 (d, J = 7.3 Hz, =CH, 1H), 7.45 (d, J = 8.1 Hz, =CH, 1H), 7.36–7.31 (m, =CH, 2H), 7.16 (t, J = 7.3 Hz, =CH, 1H), 7.11 (s, =CH, 1H), 6.78–7.74 (m, =CH, 2H), 5.71 (s, NH_2, 2H); ^{13}C NMR (100 MHz, $CDCl_3$): δ 177.0, 149.7, 137.0, 135.2, 133.8, 132.5, 127.8, 126.0, 123.0, 120.9, 119.3, 117.0, 116.2, 112.0, 111.7; IR (KBr, cm^{-1}): 3437, 3401, 3038, 2918, 2876, 2851, 2725, 1725, 1635, 1424, 1205, 777; Anal. Calcd. for $C_{15}H_{12}N_2O$: C, 76.25; H, 5.12; N, 11.86; found: C, 76.37; H, 5.11; N, 11.97; TLC: R_f = 0.32 (EtOAc/hexane (v/v: 3/7), 254 nm).

3.4. The reaction of 4,7-dihydro-1*H*-indole (2, 2 equiv.) with isatin (4, 1 equiv.)

To a solution of 4,7-dihydro-1*H*-indole (**2**; 300 mg, 2.50 mmol) in MeCN (5 mL) was added isatin (**4**, 185 mg, 1.26 mmol) and $Bi(NO_3)_3 \cdot 5H_2O$ (0.1 mmol). The reaction mixture was stirred magnetically in a flask at 100 °C. The reaction was monitored by TLC. After the completion of the reaction, the mixture was diluted with ethyl acetate (30 mL) and washed with water (2 × 50 mL), and the organic phase was dried over Na_2SO_4. The crude product was dissolved in CH_2Cl_2 (15 mL) and *p*-benzoquinone (330 mg, 3.06 mmol) was added. The mixture was stirred at room temperature overnight. After completion of the reaction, the solvent was evaporated, the crude product was dissolved with ethyl acetate (30 mL), and the organic phase was washed with NaOH (2 N, 2 × 30 mL) and brine (30 mL) and dried over Na_2SO_4. The crude product was purified by silica gel column chromatography and isolated compounds was given according to elution sequence (EtOAc/hexane; v/v: 3/17). After purification, 1*H*,1″*H*-[2,3′:3′,2″-terindol]-2′(1′*H*)-one (**12,** 382 mg, 85%) was obtained as a pale red solid (mp: 137–138 °C (crystallized over CH_2Cl_2/hexane)).

^{1}H NMR (400 MHz, $CDCl_3$): δ 8.76 (bs, NH, 2H), 8.30 (bs, NH, 1H), 7.60 (d, J = 7.6 Hz, =CH, 1H), 7.52 (d, J = 7.6 Hz, =CH, 2H), 7.33–7.26 (m, =CH, 3H), 7.20–7.13 (m, =CH, 3H), 7.06 (t, J = 7.6 Hz, =CH, 2H), 6.99 (d, J = 7.6 Hz, =CH, 1H), 6.42 (s, =CH, 2H); ^{13}C NMR (100 MHz, $CDCl_3$): δ 177.0, 140.3, 136.8, 135.1, 130.8, 129.4, 128.0, 126.1, 123.6, 122.7, 120.9, 120.4, 111.4, 110.9, 102.4, 79.3; IR (KBr, cm^{-1}): 3451,

3195, 3115, 3061, 2816, 1760, 1738, 1698, 1589, 1270, 1203, 1145, 887, 870, 770; Anal. Calcd. for $C_{24}H_{17}N_3O$: C, 79.32; H, 4.72; N, 11.56, found: C, 79.57; H, 4.51; N, 11.31; TLC: R_f = 0.16 (EtOAc/hexane (v/v: 3/17), 254 nm).

3.5. Preparation of hemolysate

Fresh blood samples were obtained from rats and placed in EDTA-containing tubes. In order to distinguish erythrocytes from plasma, blood samples were filtered to remove any impurities, then centrifuged for 15 min at 2500 × g to remove plasma. After that the precipitated erythrocytes were washed three times with 0.16 M KCl and hemolyzed with 5 volumes of cold water. Then, to remove the cell membranes and intact cells, 30 min of centrifugation at 10,000 × g was performed.

3.6. 2′,5′-ADP Sepharose 4B Affinity chromatography

Following preparation of the hemolysate, the sample was passed through a 2′,5′-ADP Sepharose 4B Affinity column, which was equilibrated with 50 mM KH_2PO_4, 1 mM EDTA, and 1 mM DTT at pH 7.3. The protein was eluted with 80 mM KH_2PO_4, 10 mM EDTA, 80 mM KCI, and 5 mM $NADP^+$ at pH 7.3. All procedures were carried out at 4 °C.[41–43]

3.7. In vitro enzyme inhibition studies

G6PD and 6PGD enzyme activities were measured at 25 °C spectrometrically at 340 nm by following the rate of appearance of NADPH. Assays were initiated by the addition of enzyme to 1.0 mL of 100 mM Tris-HCl, pH 8, containing 0.5 mM EDTA, 0.01 mM $MgCl_2$, 0.6 mM G6P/6PGA, and 0.2 mM $NADP^+$. To determine the effect of compounds **5**, **7**, and **12** on the activity of rat erythrocyte G6PD and 6PGD, different concentrations of the corresponding compounds were added in the assay mixture given above. The enzyme activities in the absence of compounds were taken as 100%. Activity % vs. compound concentration graphs were drawn and used to calculate the drug concentrations causing a 50% decrease in enzyme activity (IC_{50} values). The types of inhibition and K_i constants were determined via Lineweaver–Burk graphs.

3.8. Structure preparation, homology modeling, and ligand docking

The sequences of G6PD and 6PGD of rat erythrocytes were retrieved from UniProt (http://www.uniprot.org/uniprot) in the FASTA format. The sequences were then submitted to PHYRE2 (Protein Homology/analogy Recognition Engine V 2.0) for protein structure prediction.[49] The X-ray crystal structures of human G6PD (PDB-ID: 1QKI) and sheep 6PGD (PDB-ID: 1PGP) were used as starting structures for molecular modeling. PROCHECK[48] was used for model validation. The molecular structure of compound 5 was built in Chem3D Pro 12.0 and energy-minimized prior to docking studies. Ligand docking calculations were performed in SwissDock.[49] The docked structures were examined manually and the best pose for the inhibitor was selected on the basis of the DG value, the scaffold conformation, and the hydrogen bonds formed between residues and the inhibitor. Estimated DG values for each docking cluster are given in Table S1. UCSF Chimera and PyMol were used for molecular visualization.[50,51]

Acknowledgements

The authors are indebted to the Department of Chemistry at Bingöl University (BAP-209-324-2015) and would also like to thank Prof Dr Nurullah Saraçoğlu for practical support and helpful discussions.

References

1. Humphrey, G. R.; Kuethe, J. T. *Chem. Rev.* **2006**, *106*, 2875-2911.
2. Cacchi, S.; Fabrizi, G. *Chem. Rev.* **2005**, *105*, 2873-2920.
3. Kamal, A.; Srikanth, Y. V. V.; Khan, M. N. A.; Shaik, T. B.; Ashraf, M. *Bioorg. Med. Chem. Lett.* **2010**, *20*, 5229-5231.
4. Sayed, M. T.; Mahmoud, K.; Hilgeroth, A.; Fakhr, I. M. I. *J. Heterocyclic Chem.* **2016**, *53*, 188-196.
5. Huber, K.; Schemies, J.; Uciechowska, U.; Wagner, J. M.; Rumpf, T.; Lewrick, F.; Süss, R.; Sippl, W.; Jung, W.; Bracher, F. *J. Med. Chem.* **2010**, *53*, 1383-1386.
6. Giannini, G.; Marzi, M.; Marzo, M. D.; Battistuzzi, G.; Pezzi, R.; Brunetti, T. *Bioorg. Med. Chem. Lett.* **2009**, *19*, 2840-2844.
7. Gaisina, I. N.; Gallier, F.; Ougolkov, A. V.; Kim, K. H.; Kurome, T.; Guo, S.; Holzle, D.; Luchini, D. N.; Blond, S. Y.; Billadeau, D. D. et al. *J. Med. Chem.* **2009**, *52*, 1853-1863.
8. Paira, P.; Hazra, A.; Kumar, S.; Paira, R.; Sahu, K. B.; Naskar, S.; Saha, P.; Mondal, S.; Maity, A.; Banerjee, S. et al. *Bioorg. Med. Chem. Lett.* **2009**, *19*, 4786-4789.
9. Shiri, M.; Zolfigol, M. A.; Kruger, H. G.; Tanbakouchian, Z. *Chem. Rev.* **2010**, *110*, 2250-2293.
10. Safe, S.; Papineni, S.; Chintharlapalli, S. *Cancer Lett.* **2008**, *269*, 326-338.
11. Lee, J. Y.; Lee, M. H.; Jeong, K. S. *Supramol. Chem.* **2007**, *19*, 257-263.
12. Chmielewski, M. J.; Charon, M.; Jurczak, J. *Org. Lett.* **2004**, *6*, 3501-3504.
13. Kilic, H.; Aydin, O.; Bayindir, S.; Saracoglu, N. J. Heterocyclic Chem. 2016, 53, 2096-2101.
14. Hong, L.; Liu, C.; Sun, W.; Wang, L.; Wong, K.; Wang, R. *Org. Lett.* **2009**, *10*, 2177-2180.
15. Gao, J.; Shao, Y.; Zhu, J.; Zhu, J.; Mao, H.; Wang, X.; Lv, J. *Org. Chem.* **2014**, *79*, 9000-9008.
16. Zhao, F.; Zhang, D.; Nian, Y.; Zhang, L.; Yang W.; Liu, H. *Org. Lett.* **2014**, *16*, 5124-5127.
17. Lu, B. Z.; Wei, H. X.; Zhang, Y.; Zhao, W.; Dufour, M.; Li, G.; Farina, V.; Senanayake, C. H. *J. Org. Chem.* **2013**, *78*, 4558-4562.
18. Gogoi, A.; Guin, S.; Rout, S. K.; Patel, B. K. *Org. Lett.* **2013**, *15*, 1802-1805.
19. Prasad, B.; Adepu, R.; Sandra, S.; Rambabu, D.; Krishna, G. R.; Reddy, C. M.; Deora, G. S.; Misra, P.; Pal, M. *Chem. Commun.* **2012**, *48*, 10434-10436.
20. Bayindir, S.; Erdogan, E.; Kilic, H.; Saracoglu, N. *Synlett* **2010**, *10*, 1455-1458.
21. Kilic, H.; Bayindir, S.; Erdogan, E.; Saracoglu, N. *Tetrahedron* **2012**, *68*, 5619-5630.
22. Bayindir, S.; Erdogan, E.; Kilic, H.; Aydin, O.; Saracoglu, N. *J. Heterocyclic Chem.* **2015**, *52*, 1589-1594.
23. Aydin, O.; Kilic, H.; Bayindir, S.; Saracoglu, N. *J. Heterocyclic Chem.* **2016**, *53*, 1540-1553.
24. Kilic, H.; Bayindir, S.; Erdogan, E.; Agopcan, C. S.; Konuklar, F. A. S.; Bali, S. K.; Saracoglu, N.; Aviyente, V. *New J. Chem.* **2017**, *41*, 9674-9687.
25. Çavdar, H.; Saraçoğlu, N. *Tetrahedron* **2005**, *61*, 2401-2405.
26. Çavdar, H.; Saraçoğlu, N. *J. Org. Chem.* **2006**, *71*, 7793-7799.
27. Kilic, H.; Bayindir, S.; Saracoglu, N. *Curr. Org. Chem.* **2014**, *11*, 167-181.

28. Bayindir, S.; Saracoglu, N. *RSC Adv.* **2016**, *6*, 72959-72967.
29. Wang, L. T.; He, X. M.; Guo, Y.; Xu, J. A.; Shao, S. J. *Org. Biomol. Chem.* **2011**, *9*, 752-757.
30. Gale, P. A.; Garrido, S. E. G.; Garric, J. *Chem. Soc. Rev.* **2008**, *37*, 151-190.
31. Ghosh, K.; Kar, D.; Joardar, S.; Samander, A.; Bukhsh, A. R. K. *RSC Adv.* **2014**, *4*, 11590-11597.
32. Talaz, O.; Cavdar, H.; Durdagi, S.; Azak, H.; Ekinci, D. *Bioorg. Med. Chem.* **2013**, *21*, 1477-1482.
33. Gupte, S. A. *Curr. Opin. Investig Drugs* **2008**, 9, 993-1000.
34. Beutler, E. *N. Engl. J. Med.* **1991**, *324*, 169-174.
35. Kovarova, J.; Barrett, M.P. *Trends Parasitol.* **2016**, *32*, 8, 622-634.
36. Krebs, H. A.; Eggleston, L. V. *Adv. Enzyme Regul.* **1978**, *12*, 421-433.
37. Zhang, C.; Zhang, Z.; Zhu, Y.; Qin, S. *Anticancer Agents Med. Chem.* **2014**, *14*, 280-289.
38. Park, J.; Rho, H. K.; Kim, K. H.; Choe, S. S.; Lee, Y. S.; Kim, J. B. *Mol. Cell Biol.* **2005**, *25*, 5146-5157.
39. Park, J.; Choe, S. S.; Choi, A. H.; Kim, K. H.; Yoon, M. J.; Suganami, T.; Ogawa, Y.; Kim, J. B. *Diabetes* **2006**, *55*, 2939-2949.
40. Lin, R.; Elf, S.; Shan, C.; Kang, H. B.; Ji, Q.; Zhou, L.; Hitosugi, T.; Zhang, L.; Zhang, S.; Seo, J. H. et al. *Nat. Cell Biol.* **2015**, *17*, 1484-1496.
41. Ozmen, I.; Kufrevioglu, O. I.; Gul, M. *Drug Chem. Toxicol.* 2005, *28*, 433-445.
42. Temel, Y.; Kocyigit, U. M. *J. Biochem Mol Toxicol.* **2017**, *31*, 21927-21931.
43. Beydemir, S.; Ciftci, M.; Yılmaz, H.; Küfrevioglu, O. I. *Turk. J. Vet. Anim. Sci.* **2004**, *28*, 707-714.
44. Adams, M. J.; Ellis, G. H.; Gover, S.; Naylor, C. E.; Phillips, C. *Structure* **1994**, *2*, 651-668.
45. Zhang, L.; Chooback, L.; Cook, P. F. *Biochem. J.* **1999**, *38*, 11231-11238.
46. Karsten, W. E.; Chooback, L.; Cook, P. F. *Biochem. J.* **1998**, *37*, 15691-15697.
47. Kelley, L. A.; Mezulis, S.; Yates, C. M.; Wass, M. N.; Sternberg, M. J. *Nat Protoc.* **2015**, *10*, 845-858.
48. Laskowski, R. A.; MacArthur, M. W.; Moss, D. S.; Thornton, J. M. *J. App. Cryst.* **1993**, *26*, 283-291.
49. Grosdidier, A.; Zoete, V.; Michielin, O. *Nucleic Acids Res.* **2011**, *39*, 270-277.
50. Pettersen, E. F.; Goddard, T. D.; Huang, C. C.; Couch, G. S.; Greenblatt, D. M.; Meng, E. C.; Ferrin, T. E. *J Comput Chem.* **2004**, *25*, 1605-1612.
51. Delano, W. L. *The PyMOL Molecular Graphics System*; Schrödinger: Cambridge, MA, USA, 2002.

Supporting Information

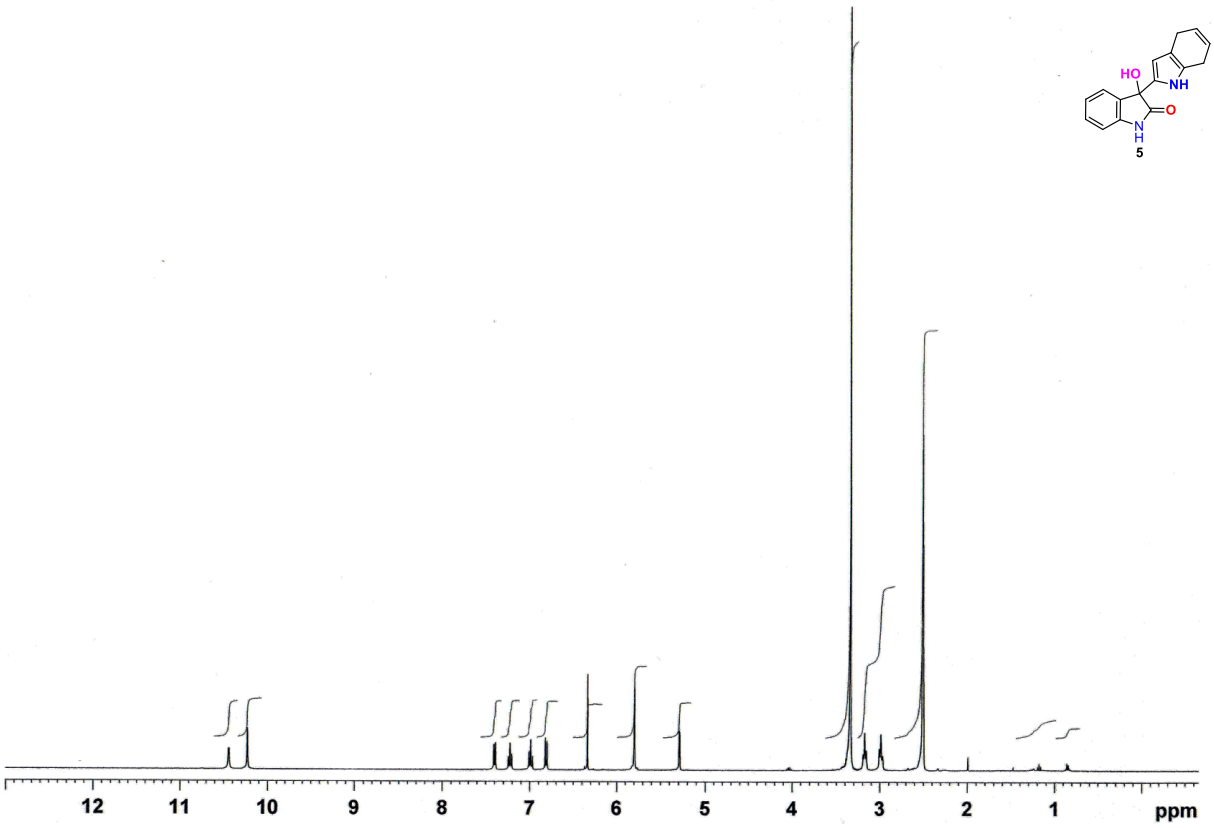

Figure S1. ^{1}H NMR (400 MHz) spectra of 3-(4,7-dihydro-1*H*-indol-2-yl)-3-hydroxyindolin-2-one (**5**) (DMSO-d6).

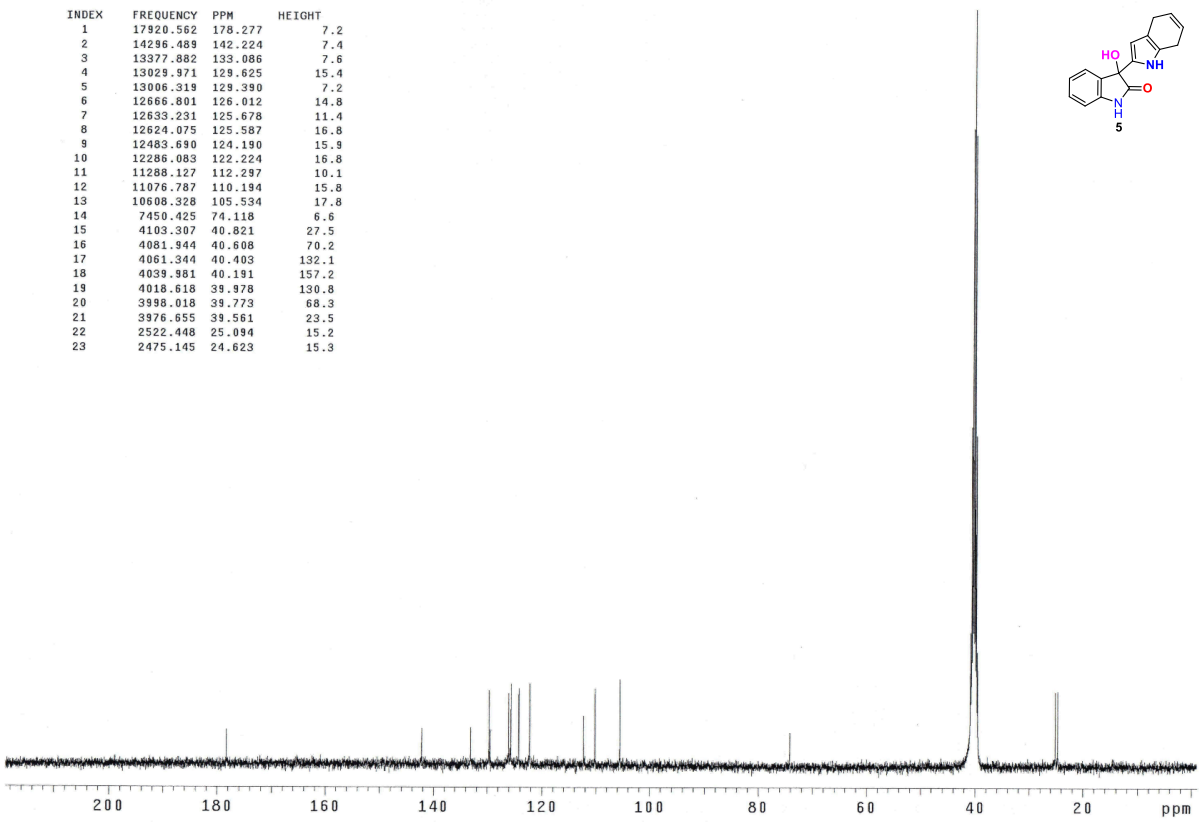

INDEX	FREQUENCY	PPM	HEIGHT
1	17920.562	178.277	7.2
2	14296.489	142.224	7.4
3	13377.882	133.086	7.6
4	13029.971	129.625	15.4
5	13006.319	129.390	7.2
6	12666.801	126.012	14.8
7	12633.231	125.678	11.4
8	12624.075	125.587	16.8
9	12483.690	124.190	15.9
10	12286.083	122.224	16.8
11	11288.127	112.297	10.1
12	11076.787	110.194	15.8
13	10608.328	105.534	17.8
14	7450.425	74.118	6.6
15	4103.307	40.821	27.5
16	4081.944	40.608	70.2
17	4061.344	40.403	132.1
18	4039.981	40.191	157.2
19	4018.618	39.978	130.8
20	3998.018	39.773	68.3
21	3976.655	39.561	23.5
22	2522.448	25.094	15.2
23	2475.145	24.623	15.3

Figure S2. ^{13}C NMR (100 MHz) spectra of 3-(4,7-dihydro-1*H*-indol-2-yl)-3-hydroxyindolin-2-one (**5**) (DMSO-d6).

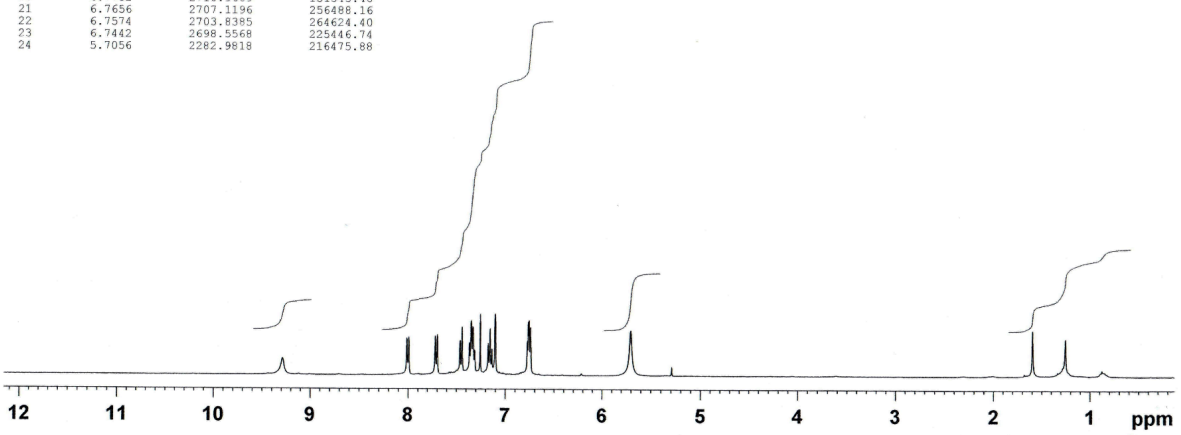

Peak	?(F1) [ppm]	?(F1) [Hz]	Intensity [abs]
1	9.2898	3717.1278	80046.32
2	8.0145	3206.8420	178510.33
3	8.0119	3205.8016	172539.76
4	7.9942	3198.7193	182863.82
5	7.7200	3089.0037	183766.11
6	7.7000	3081.0011	190494.31
7	7.4631	2986.2103	166602.57
8	7.4424	2977.9276	232124.31
9	7.3640	2946.5574	156491.73
10	7.3480	2940.1553	264632.37
11	7.3314	2933.5132	234177.55
12	7.3285	2932.3528	223664.72
13	7.3140	2926.5509	122007.58
14	7.3110	2925.3505	111643.86
15	7.2543	2902.6631	294997.15
16	7.1747	2870.8128	153390.86
17	7.1557	2863.2103	218598.99
18	7.1372	2855.8079	125969.59
19	7.1038	2842.4436	295888.10
20	6.7752	2710.9609	151343.48
21	6.7656	2707.1196	256488.16
22	6.7574	2703.8385	264624.40
23	6.7442	2698.5568	225446.74
24	5.7056	2282.9818	216475.88

Figure S3. ^{1}H NMR (400 MHz) spectra of (2-aminophenyl)(1H-indol-2-yl)methanone (**7**) ($CDCl_3$).

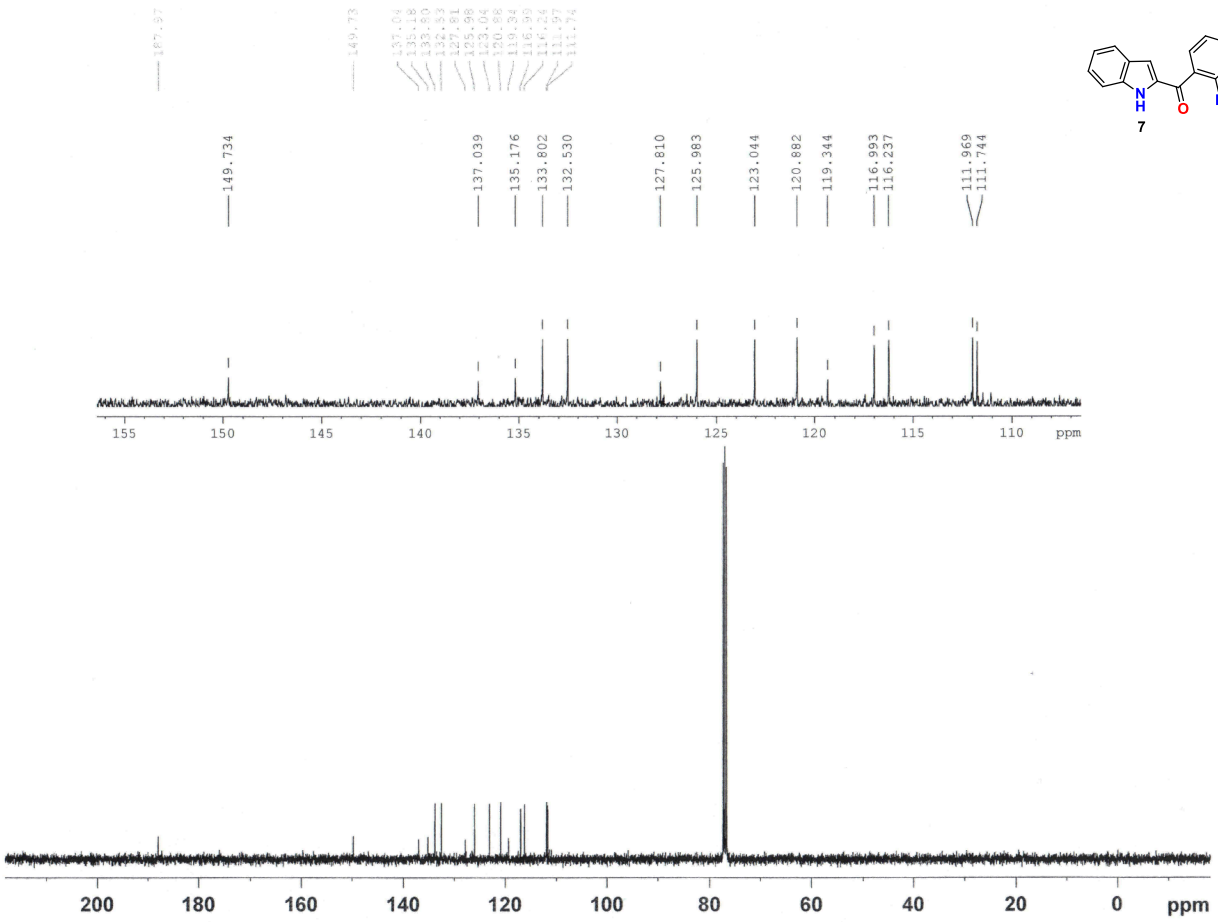

Figure S4. ^{13}C NMR (100 MHz) spectra of (2-aminophenyl)(1H-indol-2-yl)methanone (**7**) ($CDCl_3$).

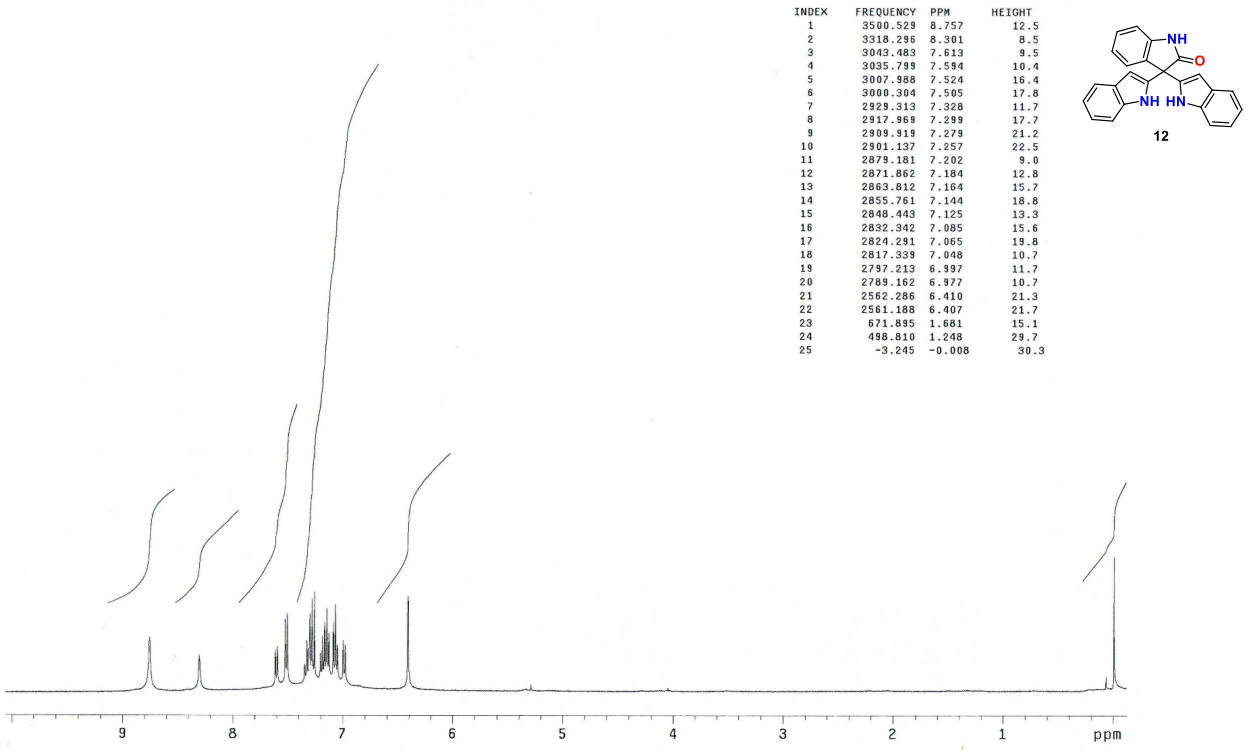

Figure S5. ^{1}H NMR (400 MHz) spectra of [2,3':3',2"-terindolin]-2'-one (**12**) ($CDCl_3$).

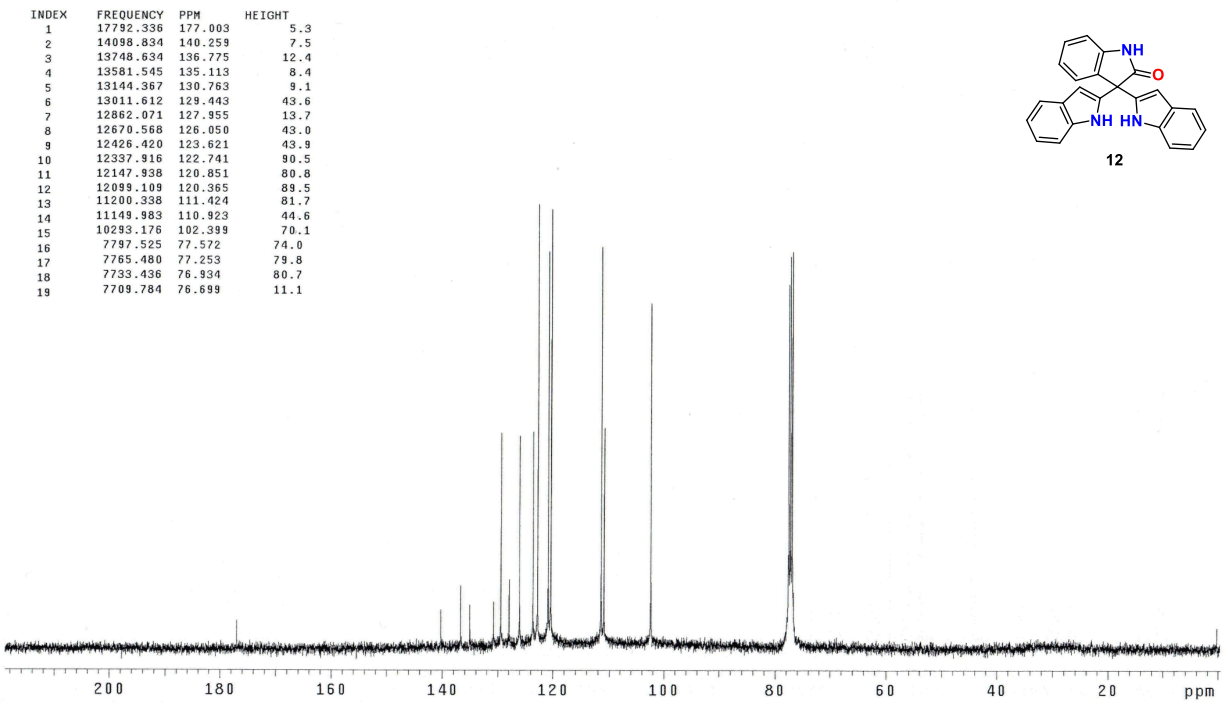

Figure S6. ^{13}C NMR (100 MHz) spectra of [2,3':3',2"-terindolin]-2'-one (**12**) ($CDCl_3$).

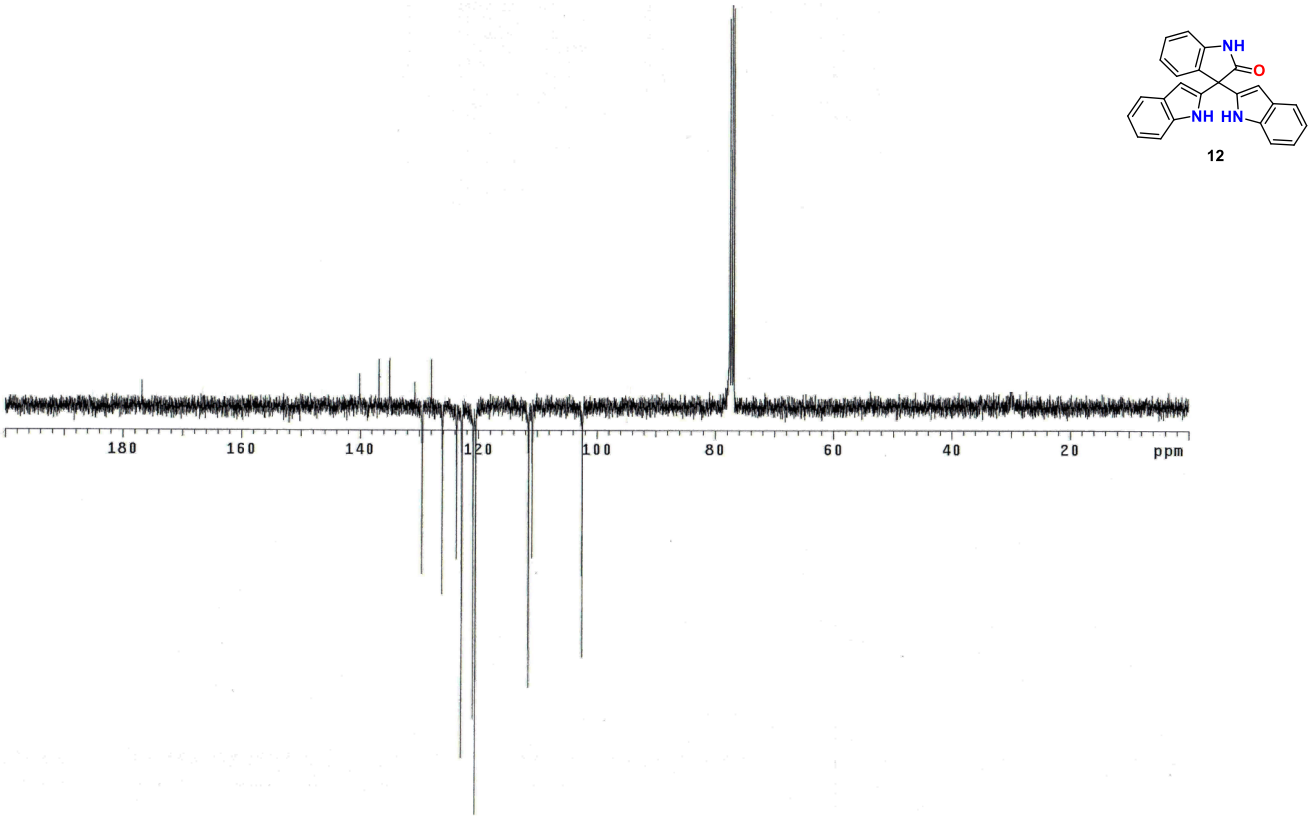

Figure S7. APT NMR (100 MHz) spectra of [2,3':3',2"-terindolin]-2'-one (**12**) ($CDCl_3$).

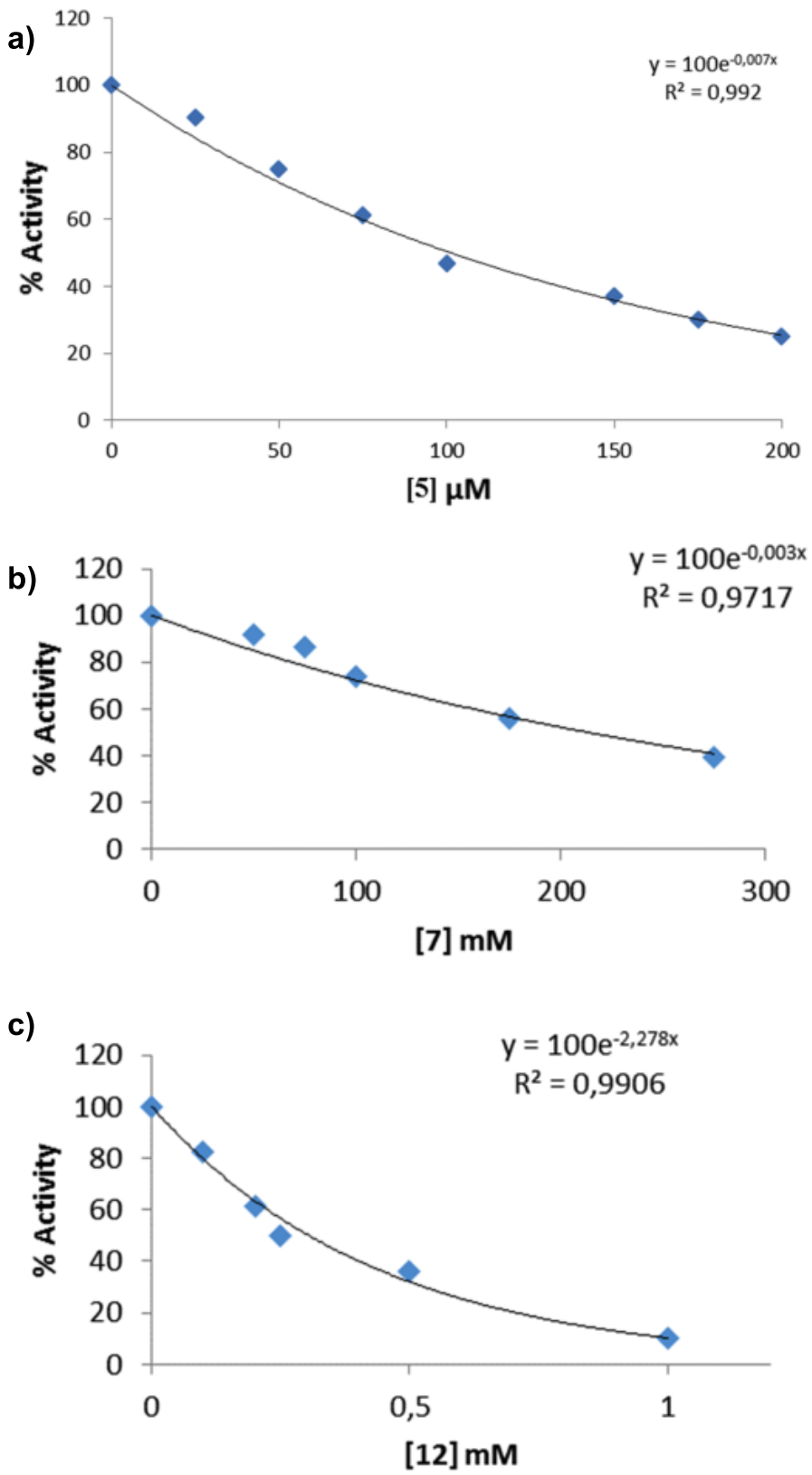

Figure S8. In vitro effect of **5** (a), **7** (b), and **12** (c) on rat erythrocyte G6PD with corresponding IC_{50} graphs.

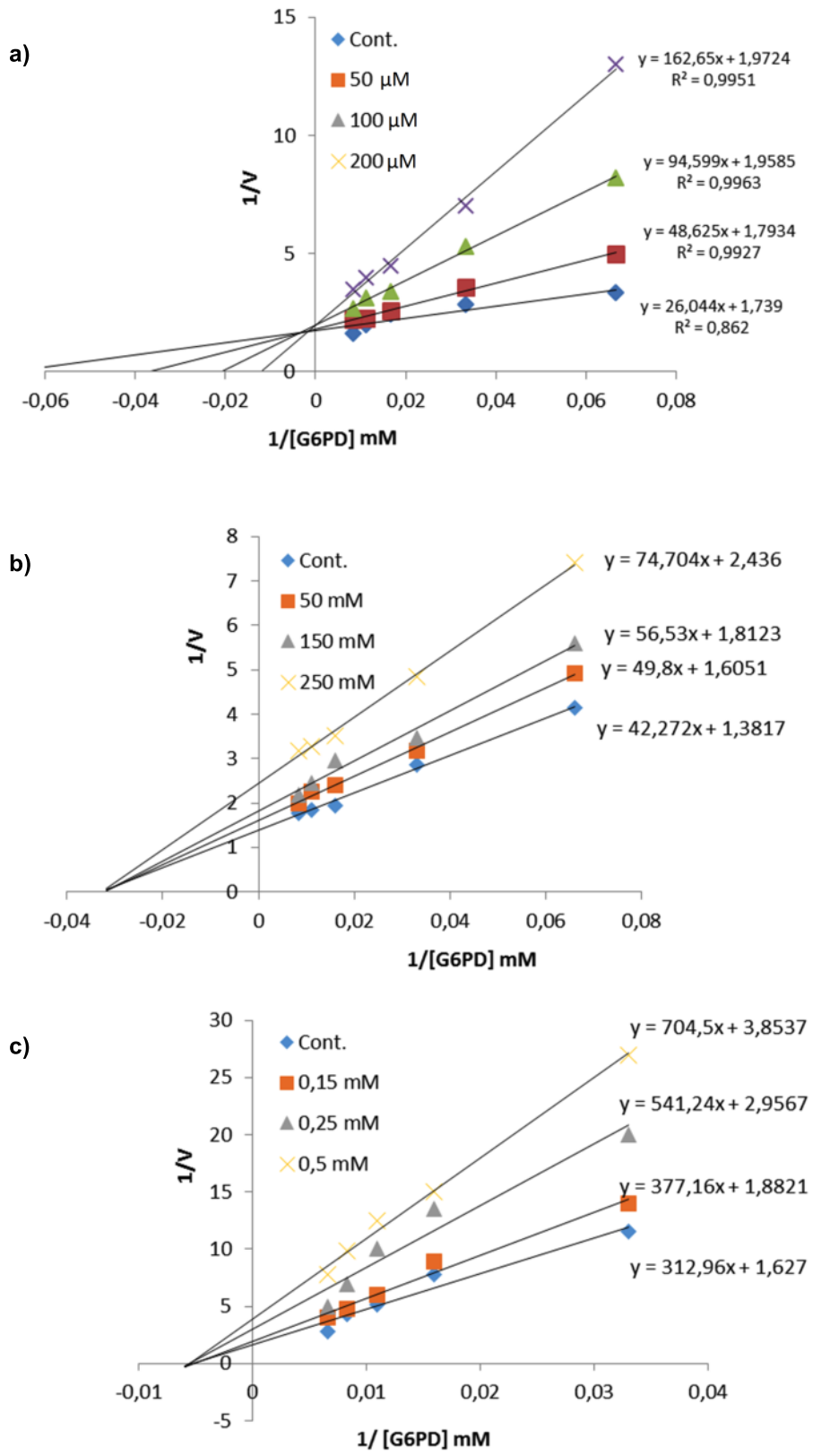

Figure S9. Lineweaver–Burk double reciprocal plot of initial velocity against G6PD and inhibitors **5** (a), **7** (b), and **12** (c) at different concentrations.

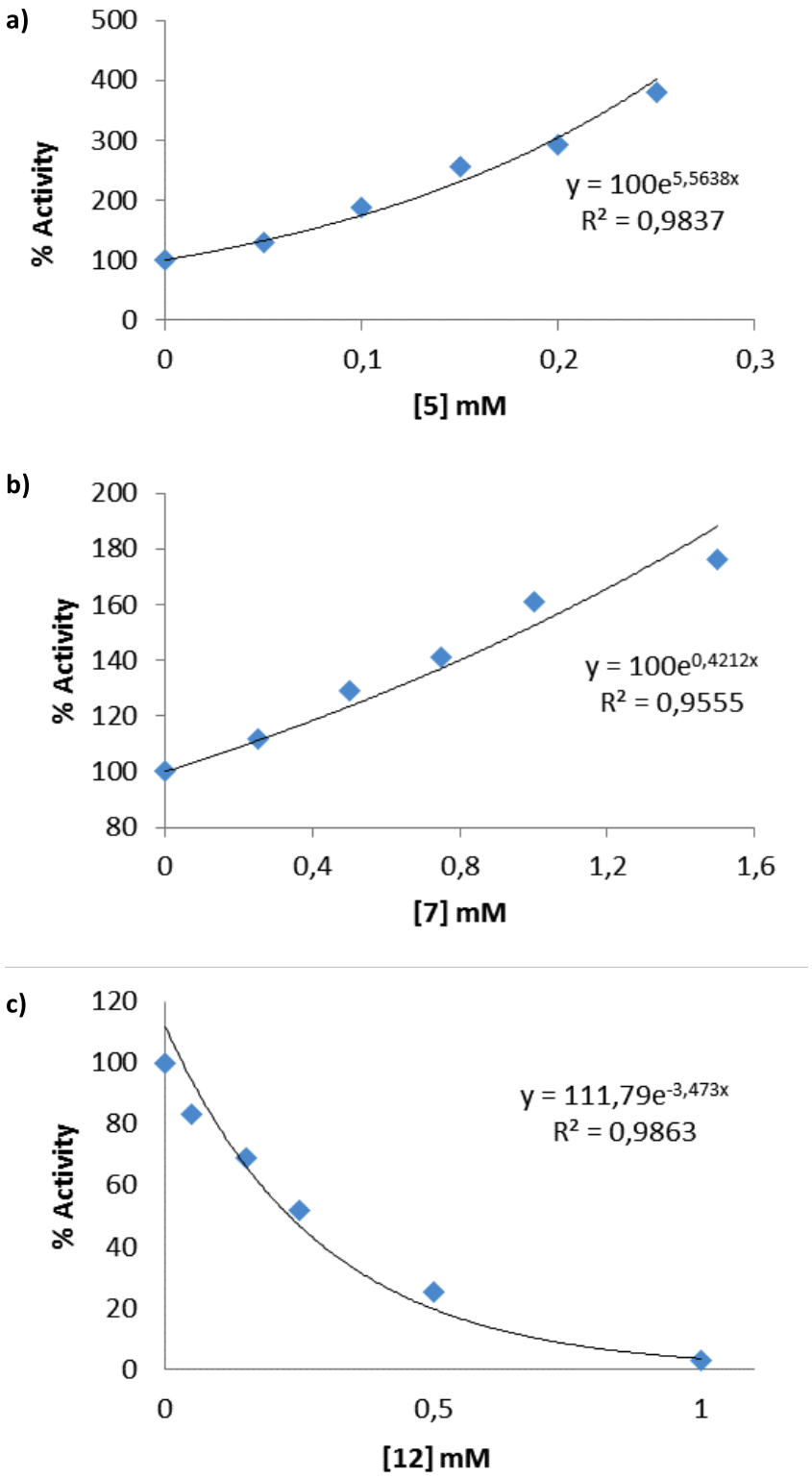

Figure S10. In vitro effect of compounds **5** (a), **7** (b), and **12** (c) on rat erythrocyte 6PGD with corresponding IC_{50} (c) and activation graphs (a and b).

a)

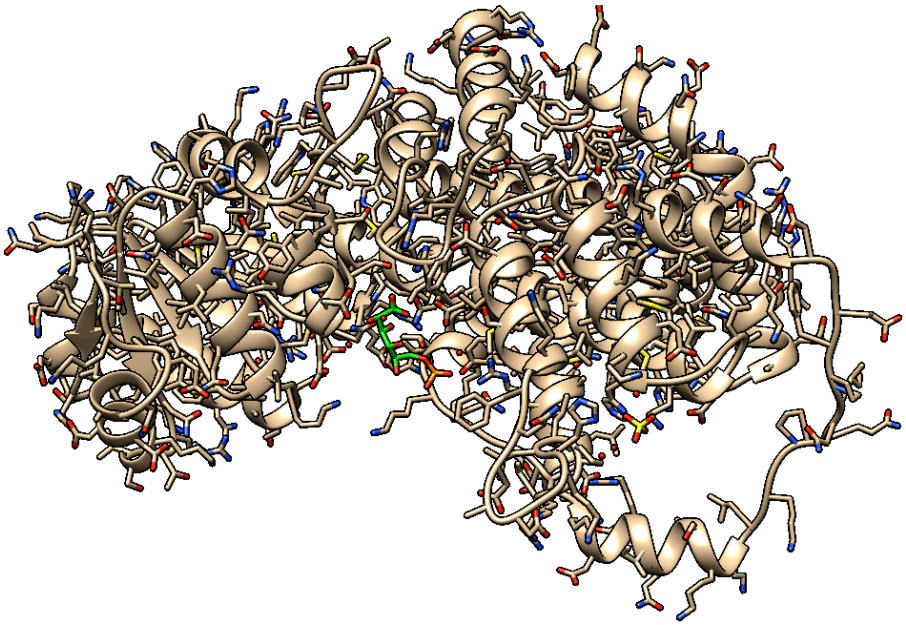

b)

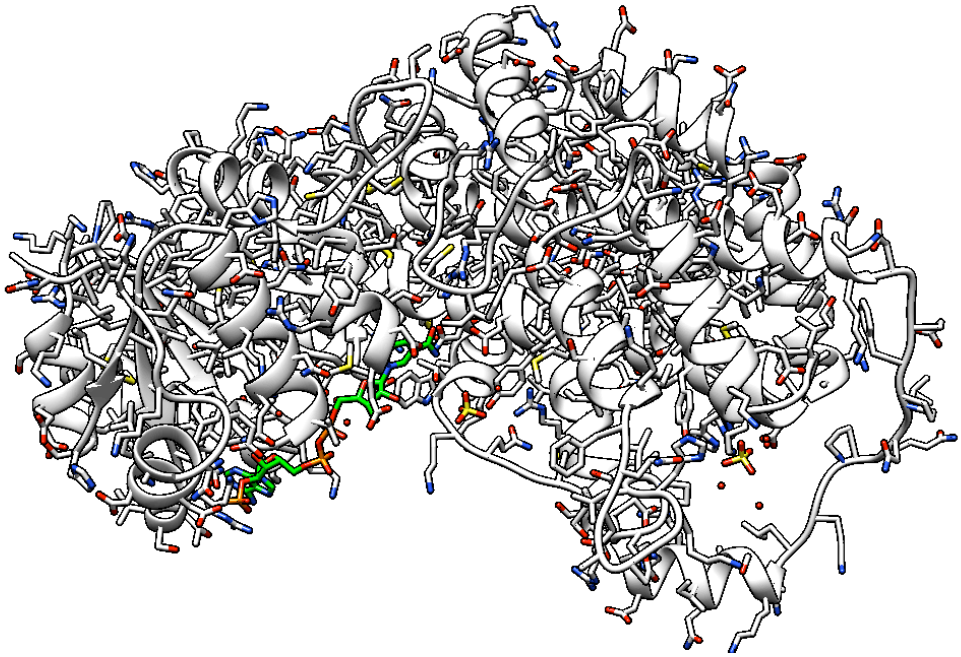

Figure S11. Representation of full view of a) $NADP^+$ (PDB-ID: 1PGN) and b) 6PGA (PDB-ID: 1PGP) binding sites in 6PGD.

Table S1. Estimated DG values for each docking cluster calculated for G6PD.

how	Cluster	Element	FullFitness (kcal/mol)	Estimated ΔG (kcal/mol)
○	0	0	-2620.43	-6.30
○	0	1	-2620.43	-6.30
○	0	2	-2620.43	-6.30
○	0	3	-2620.40	-6.31
○	0	4	-2620.26	-6.31
○	0	5	-2620.26	-6.31
○	0	6	-2619.16	-6.23
○	0	7	-2618.84	-6.21
○	1	0	-2619.60	-6.36
○	1	1	-2619.60	-6.36
○	1	2	-2619.59	-6.36
○	1	3	-2617.35	-6.22
○	1	4	-2617.30	-6.21
○	1	5	-2617.18	-6.20
○	1	6	-2616.77	-6.08
○	1	7	-2616.76	-6.08
◉	1	8	-2616.76	-6.08
○	1	9	-2616.73	-6.23
○	1	10	-2616.65	-6.23
○	1	11	-2614.18	-5.92
○	1	12	-2614.12	-5.91
○	1	13	-2612.90	-5.85
○	1	14	-2612.90	-5.84
○	1	15	-2612.89	-5.84
○	2	0	-2619.18	-6.19
○	2	1	-2619.17	-6.19
○	2	2	-2619.09	-6.19
○	2	3	-2619.09	-6.19

how	Cluster	Element	FullFitness (kcal/mol)	Estimated ΔG (kcal/mol)
○	2	4	-2618.66	-6.21
○	2	5	-2617.19	-6.06
○	2	6	-2617.14	-6.04
○	2	7	-2617.14	-6.04
○	3	0	-2619.08	-6.73
○	3	1	-2619.06	-6.73
○	3	2	-2619.05	-6.73
○	3	3	-2619.04	-6.73
○	3	4	-2619.03	-6.73
○	3	5	-2618.35	-6.68
○	3	6	-2613.98	-6.23
○	3	7	-2613.81	-6.21
○	4	0	-2618.88	-6.42
○	4	1	-2618.67	-6.41
○	4	2	-2618.67	-6.41
○	4	3	-2618.52	-6.39
○	4	4	-2618.52	-6.39
○	4	5	-2618.18	-6.37
○	4	6	-2618.17	-6.36
○	4	7	-2617.98	-6.36
○	5	0	-2618.68	-6.43
○	5	1	-2618.63	-6.43
○	5	2	-2618.43	-6.28
○	5	3	-2618.43	-6.28
○	5	4	-2618.43	-6.28
○	5	5	-2618.42	-6.28
○	5	6	-2618.34	-6.43
○	5	7	-2618.29	-6.27
○	6	0	-2618.29	-6.24

how	Cluster	Element	FullFitness (kcal/mol)	Estimated ΔG (kcal/mol)
○	6	1	-2618.26	-6.23
○	6	2	-2617.99	-6.43
○	6	3	-2617.96	-6.42
○	6	4	-2617.82	-6.40
○	6	5	-2617.64	-6.39
○	6	6	-2617.30	-6.30
○	6	7	-2616.59	-6.21
○	7	0	-2618.16	-6.11
○	7	1	-2618.16	-6.11
○	7	2	-2618.14	-6.11
○	7	3	-2618.14	-6.11
○	7	4	-2616.94	-6.02
○	7	5	-2616.71	-5.99
○	7	6	-2616.71	-5.99
○	7	7	-2616.36	-5.95
○	8	0	-2618.03	-6.03
○	8	1	-2617.95	-6.03
○	8	2	-2617.95	-6.03
○	8	3	-2617.95	-6.03
○	8	4	-2617.95	-6.03
○	8	5	-2617.69	-6.01
○	8	6	-2617.69	-6.01
○	8	7	-2617.69	-6.01
○	9	0	-2617.74	-6.21
○	9	1	-2617.74	-6.21
○	9	2	-2617.74	-6.21
○	9	3	-2617.73	-6.20
○	9	4	-2617.73	-6.20
○	9	5	-2617.72	-6.20

how	Cluster	Element	FullFitness (kcal/mol)	Estimated ΔG (kcal/mol)
○	9	6	-2617.72	-6.20
○	9	7	-2617.72	-6.20
○	10	0	-2617.56	-6.04
○	10	1	-2617.02	-6.04
○	10	2	-2617.02	-6.04
○	10	3	-2616.98	-6.02
○	10	4	-2616.98	-6.02
○	10	5	-2616.98	-6.02
○	10	6	-2616.98	-6.02
○	10	7	-2616.98	-6.02
○	11	0	-2617.32	-5.90
○	11	1	-2617.32	-5.90
○	11	2	-2617.32	-5.90
○	11	3	-2617.08	-5.87
○	11	4	-2617.08	-5.87
○	11	5	-2616.86	-5.85
○	11	6	-2616.86	-5.85
○	11	7	-2616.86	-5.85
○	12	0	-2617.30	-6.80
○	12	1	-2617.30	-6.80
○	12	2	-2617.30	-6.80
○	12	3	-2617.29	-6.79
○	12	4	-2617.29	-6.79
○	12	5	-2617.29	-6.79
○	12	6	-2617.29	-6.79
○	12	7	-2617.27	-6.79
○	13	0	-2617.27	-6.16
○	13	1	-2617.27	-6.16
○	13	2	-2617.17	-6.14

how	Cluster	Element	FullFitness (kcal/mol)	Estimated ΔG (kcal/mol)
○	13	3	-2617.17	-6.14
○	13	4	-2617.17	-6.14
○	13	5	-2617.14	-6.14
○	13	6	-2617.14	-6.14
○	13	7	-2617.14	-6.14
○	14	0	-2616.91	-5.87
○	14	1	-2616.91	-5.87
○	14	2	-2616.91	-5.87
○	14	3	-2616.91	-5.87
○	14	4	-2616.79	-5.87
○	14	5	-2616.29	-5.82
○	14	6	-2616.29	-5.82
○	14	7	-2616.29	-5.82
○	15	0	-2616.85	-6.21
○	15	1	-2616.82	-6.22
○	15	2	-2616.46	-6.33
○	15	3	-2616.30	-6.33
○	15	4	-2613.90	-6.22
○	15	5	-2613.67	-6.12
○	15	6	-2613.66	-6.12
○	15	7	-2610.88	-5.85
○	16	0	-2616.77	-6.13
○	16	1	-2616.76	-6.13
○	16	2	-2616.76	-6.13
○	16	3	-2616.76	-6.13
○	16	4	-2616.76	-6.13
○	16	5	-2614.02	-6.06
○	16	6	-2613.96	-6.07
○	16	7	-2613.96	-6.07

how	Cluster	Element	FullFitness (kcal/mol)	Estimated ΔG (kcal/mol)
○	17	0	-2616.47	-5.83
○	17	1	-2616.42	-5.84
○	17	2	-2615.92	-5.81
○	17	3	-2615.55	-5.84
○	17	4	-2615.53	-5.84
○	17	5	-2609.80	-5.31
○	17	6	-2609.62	-5.29
○	18	0	-2616.39	-6.11
○	18	1	-2616.29	-6.09
○	18	2	-2616.29	-6.09
○	18	3	-2616.23	-6.09
○	18	4	-2615.20	-6.22
○	18	5	-2615.20	-6.22
○	18	6	-2614.90	-6.18
○	18	7	-2614.79	-6.18
○	19	0	-2616.05	-6.09
○	19	1	-2616.05	-6.09
○	19	2	-2616.01	-6.09
○	19	3	-2616.01	-6.09
○	19	4	-2616.01	-6.09
○	19	5	-2615.98	-6.09
○	19	6	-2615.98	-6.09
○	19	7	-2615.98	-6.09
○	20	0	-2615.99	-5.78
○	20	1	-2615.99	-5.78
○	20	2	-2615.99	-5.78
○	20	3	-2615.98	-5.77
○	20	4	-2615.98	-5.77
○	20	5	-2615.98	-5.77

how	Cluster	Element	FullFitness (kcal/mol)	Estimated ΔG (kcal/mol)
○	20	6	-2615.98	-5.77
○	20	7	-2615.52	-5.79
○	21	0	-2615.99	-6.32
○	21	1	-2615.99	-6.32
○	21	2	-2615.96	-6.32
○	21	3	-2615.96	-6.32
○	21	4	-2615.96	-6.32
○	21	5	-2615.96	-6.32
○	21	6	-2615.58	-6.31
○	21	7	-2615.58	-6.31
○	22	0	-2615.69	-5.77
○	22	1	-2615.69	-5.77
○	22	2	-2615.69	-5.77
○	22	3	-2615.59	-5.78
○	22	4	-2615.59	-5.78
○	22	5	-2615.59	-5.78
○	22	6	-2615.55	-5.78
○	22	7	-2615.55	-5.78
○	23	0	-2615.50	-5.93
○	23	1	-2615.50	-5.93
○	23	2	-2615.50	-5.93
○	23	3	-2615.49	-5.93
○	23	4	-2615.49	-5.93
○	23	5	-2615.49	-5.93
○	23	6	-2615.48	-5.93
○	23	7	-2615.48	-5.93
○	24	0	-2615.33	-5.86
○	24	1	-2615.33	-5.86
○	24	2	-2615.29	-5.85

how	Cluster	Element	FullFitness (kcal/mol)	Estimated ΔG (kcal/mol)
○	24	3	-2615.29	-5.85
○	24	4	-2615.09	-5.83
○	24	5	-2615.09	-5.83
○	24	6	-2615.09	-5.83
○	24	7	-2615.09	-5.83
○	25	0	-2615.22	-6.55
○	25	1	-2615.15	-6.55
○	25	2	-2615.15	-6.55
○	25	3	-2615.13	-6.54
○	25	4	-2615.13	-6.54
○	25	5	-2614.84	-6.44
○	25	6	-2614.74	-6.45
○	25	7	-2614.68	-6.45
○	26	0	-2614.97	-5.78
○	26	1	-2614.97	-5.78
○	26	2	-2614.96	-5.79
○	26	3	-2614.96	-5.79
○	26	4	-2614.96	-5.79
○	26	5	-2614.84	-5.78
○	26	6	-2614.84	-5.78
○	26	7	-2614.84	-5.78
○	27	0	-2614.94	-5.87
○	27	1	-2614.93	-5.87
○	27	2	-2614.93	-5.87
○	27	3	-2614.80	-5.85
○	27	4	-2614.80	-5.85
○	27	5	-2614.80	-5.85
○	27	6	-2614.80	-5.85
○	27	7	-2614.80	-5.85

how	Cluster	Element	FullFitness (kcal/mol)	Estimated ΔG (kcal/mol)
◯	28	0	-2614.90	-5.69
◯	28	1	-2614.90	-5.69
◯	28	2	-2614.90	-5.69
◯	28	3	-2614.90	-5.69
◯	28	4	-2614.89	-5.69
◯	28	5	-2614.89	-5.69
◯	28	6	-2614.89	-5.69
◯	28	7	-2614.89	-5.69
◯	29	0	-2614.65	-5.69
◯	29	1	-2614.65	-5.69
◯	29	2	-2614.58	-5.70
◯	29	3	-2614.58	-5.70
◯	29	4	-2614.58	-5.70
◯	29	5	-2614.52	-5.65
◯	29	6	-2614.52	-5.65
◯	29	7	-2614.52	-5.65
◯	30	0	-2614.50	-5.87
◯	30	1	-2614.49	-5.87
◯	30	2	-2614.38	-5.70
◯	30	3	-2614.28	-5.74
◯	30	4	-2614.07	-5.69
◯	30	5	-2613.89	-5.68
◯	30	6	-2613.89	-5.68
◯	30	7	-2613.89	-5.68
◯	31	0	-2613.23	-5.67
◯	31	0	-2613.23	-5.67

Table S2. Estimated DG values for each docking cluster calculated for 6PGD.

Show	Cluster	Element	FullFitness (kcal/mol)	Estimated ΔG (kcal/mol)
○	0	0	-2341.65	-6.86
○	0	1	-2335.59	-6.39
○	0	2	-2335.36	-6.50
○	0	3	-2335.36	-6.51
○	0	4	-2335.34	-6.50
○	0	5	-2333.33	-6.38
○	0	6	-2332.03	-6.24
○	0	7	-2330.66	-6.33
○	1	0	-2340.22	-7.09
○	1	1	-2340.22	-7.09
○	1	2	-2340.21	-7.09
○	1	3	-2340.09	-7.09
○	1	4	-2339.89	-7.07
○	1	5	-2339.38	-7.15
○	1	6	-2338.94	-7.11
○	1	7	-2338.73	-7.11
○	2	0	-2338.92	-6.66
○	2	1	-2338.06	-6.54
○	2	2	-2337.34	-6.45
○	2	3	-2336.12	-6.51
○	2	4	-2336.11	-6.52
○	2	5	-2335.36	-6.53
○	2	6	-2335.35	-6.54
○	2	7	-2334.74	-6.30
○	3	0	-2338.63	-6.98
○	3	1	-2338.47	-6.97
○	3	2	-2336.69	-6.54
○	3	3	-2336.56	-6.54
○	3	4	-2335.35	-6.50
○	3	5	-2335.32	-6.48
○	3	6	-2335.27	-6.49
○	3	7	-2335.19	-6.36
○	3	8	-2335.03	-6.44
○	4	0	-2338.36	-6.78
○	4	1	-2338.20	-6.77
○	4	2	-2334.30	-6.48
○	4	3	-2334.29	-6.48
○	4	4	-2334.22	-6.46
○	4	5	-2334.17	-6.47
○	4	6	-2334.16	-6.45
○	4	7	-2329.67	-6.14
○	5	0	-2338.14	-6.55
○	5	1	-2337.47	-6.53
○	5	2	-2337.37	-6.53
○	5	3	-2337.31	-6.52
○	5	4	-2335.97	-6.54
○	5	5	-2335.59	-6.50
○	5	6	-2335.47	-6.47
○	5	7	-2335.06	-6.43
○	6	0	-2337.98	-6.84
○	6	1	-2337.98	-6.84
○	6	2	-2337.43	-6.83
○	6	3	-2337.17	-6.76
○	6	4	-2337.14	-6.76
○	6	5	-2336.96	-6.71
○	6	6	-2336.96	-6.71
○	6	7	-2336.96	-6.71

Show	Cluster	Element	FullFitness (kcal/mol)	Estimated ΔG (kcal/mol)
○	6	8	-2336.76	-6.70
○	6	9	-2336.76	-6.70
○	6	10	-2336.51	-6.67
○	6	11	-2336.44	-6.68
○	6	12	-2336.05	-6.70
○	6	13	-2336.05	-6.70
○	6	14	-2336.05	-6.70
○	6	15	-2335.64	-6.64
○	7	0	-2337.86	-6.62
○	7	1	-2337.57	-6.57
○	7	2	-2337.24	-6.78
○	7	3	-2332.61	-6.21
○	8	0	-2337.82	-6.81
○	8	1	-2337.82	-6.81
○	8	2	-2337.82	-6.81
○	8	3	-2337.81	-6.81
○	8	4	-2336.70	-6.61
○	8	5	-2336.68	-6.61
○	8	6	-2336.68	-6.61
○	8	7	-2336.68	-6.61
○	9	0	-2337.80	-6.96
○	9	1	-2337.03	-6.78
○	9	2	-2336.53	-6.78
○	9	3	-2335.81	-6.66
○	9	4	-2335.78	-6.68
○	9	5	-2335.73	-6.73
○	9	6	-2333.95	-6.49
○	10	0	-2337.79	-6.73
○	10	1	-2337.67	-6.72

Show	Cluster	Element	FullFitness (kcal/mol)	Estimated ΔG (kcal/mol)
○	10	2	-2337.67	-6.86
○	10	3	-2337.61	-6.86
○	10	4	-2337.59	-6.66
○	10	5	-2337.33	-6.46
○	10	6	-2337.26	-6.85
○	10	7	-2337.26	-6.85
○	10	8	-2336.73	-6.87
○	10	9	-2336.73	-6.87
○	10	10	-2336.65	-6.88
○	10	11	-2336.50	-6.77
○	10	12	-2336.33	-6.70
○	10	13	-2336.33	-6.67
○	10	14	-2336.26	-6.47
○	10	15	-2336.25	-6.45
○	10	16	-2334.77	-6.37
○	10	17	-2333.82	-6.29
○	11	0	-2337.58	-6.77
○	11	1	-2337.58	-6.77
○	11	2	-2337.54	-6.77
○	11	3	-2337.51	-6.74
○	11	4	-2337.50	-6.74
○	11	5	-2335.82	-6.61
○	11	6	-2335.76	-6.60
○	11	7	-2335.66	-6.59
○	12	0	-2337.46	-6.71
○	12	1	-2337.46	-6.71
○	12	2	-2337.46	-6.71
○	12	3	-2337.46	-6.71
○	12	4	-2337.45	-6.69

Show	Cluster	Element	FullFitness (kcal/mol)	Estimated ΔG (kcal/mol)
○	12	5	-2337.37	-6.70
○	12	6	-2337.37	-6.70
○	12	7	-2336.91	-6.63
○	12	8	-2336.91	-6.63
○	12	9	-2335.40	-6.43
○	12	10	-2335.38	-6.45
○	12	11	-2335.37	-6.45
○	12	12	-2335.28	-6.50
○	12	13	-2334.83	-6.44
○	12	14	-2332.94	-6.43
○	12	15	-2332.91	-6.43
○	13	0	-2337.36	-6.58
○	13	1	-2337.34	-6.57
○	13	2	-2336.97	-6.50
○	14	0	-2337.17	-6.71
○	14	1	-2336.14	-6.71
○	14	2	-2336.11	-6.70
○	14	3	-2335.49	-6.50
○	14	4	-2335.38	-6.54
○	14	5	-2334.58	-6.42
○	14	6	-2334.28	-6.61
○	14	7	-2332.27	-6.48
○	15	0	-2337.11	-6.61
○	15	1	-2337.11	-6.61
○	15	2	-2337.11	-6.61
○	15	3	-2337.11	-6.61
○	15	4	-2337.07	-6.61
○	15	5	-2337.07	-6.61
○	15	6	-2337.07	-6.61

Show	Cluster	Element	FullFitness (kcal/mol)	Estimated ΔG (kcal/mol)
○	15	7	-2336.90	-6.59
○	16	0	-2336.92	-6.70
○	16	1	-2336.14	-6.60
○	16	2	-2334.79	-6.37
○	16	3	-2334.71	-6.37
○	16	4	-2332.71	-6.41
○	16	5	-2331.48	-6.24
○	16	6	-2331.48	-6.24
○	16	7	-2331.32	-6.22
○	17	0	-2336.27	-6.46
○	18	0	-2335.85	-6.40
○	18	1	-2335.85	-6.40
○	18	2	-2335.81	-6.40
○	18	3	-2335.81	-6.40
○	18	4	-2335.77	-6.40
○	18	5	-2335.77	-6.40
○	18	6	-2335.77	-6.40
○	18	7	-2335.77	-6.40
○	19	0	-2335.74	-6.38
○	19	1	-2335.74	-6.38
○	19	2	-2335.74	-6.38
○	19	3	-2335.74	-6.38
○	19	4	-2335.74	-6.38
○	19	5	-2335.72	-6.38
○	19	6	-2335.71	-6.38
○	19	7	-2335.71	-6.38
○	19	8	-2334.70	-6.30
○	20	0	-2335.70	-6.49
○	20	1	-2335.23	-6.44

Show	Cluster	Element	FullFitness (kcal/mol)	Estimated ΔG (kcal/mol)
○	20	2	-2334.99	-6.52
○	20	3	-2334.91	-6.40
○	20	4	-2334.85	-6.41
○	20	5	-2332.37	-6.14
○	20	6	-2332.15	-6.10
○	20	7	-2331.94	-6.29
○	21	0	-2335.65	-6.40
○	22	0	-2335.46	-6.37
○	22	1	-2335.44	-6.48
○	22	2	-2335.42	-6.48
○	22	3	-2335.42	-6.48
○	22	4	-2335.42	-6.48
○	22	5	-2335.18	-6.40
○	22	6	-2335.17	-6.40
○	22	7	-2333.47	-6.34
○	23	0	-2335.27	-6.65
○	23	1	-2335.25	-6.67
○	23	2	-2335.23	-6.66
○	23	3	-2335.22	-6.66
○	23	4	-2335.22	-6.66
○	23	5	-2335.17	-6.66
○	24	0	-2335.25	-6.65
○	24	1	-2334.84	-6.51
○	24	2	-2334.82	-6.51
○	24	3	-2334.74	-6.59
○	24	4	-2334.04	-6.58
○	24	5	-2334.01	-6.58
○	24	6	-2334.01	-6.58
○	25	0	-2335.22	-6.42

Show	Cluster	Element	FullFitness (kcal/mol)	Estimated ΔG (kcal/mol)
○	25	1	-2335.22	-6.42
○	25	2	-2335.07	-6.44
○	25	3	-2334.79	-6.42
○	25	4	-2334.33	-6.24
○	25	5	-2334.33	-6.24
○	25	6	-2334.21	-6.23
○	25	7	-2334.16	-6.23
○	26	0	-2335.14	-6.65
○	26	1	-2335.13	-6.66
○	26	2	-2335.11	-6.66
○	26	3	-2332.56	-6.48
○	26	4	-2332.54	-6.47
○	26	5	-2332.04	-6.36
○	26	6	-2331.99	-6.39
○	26	7	-2331.84	-6.41
○	27	0	-2334.98	-6.33
○	27	1	-2334.98	-6.33
○	27	2	-2334.98	-6.32
○	27	3	-2334.96	-6.33
○	27	4	-2334.96	-6.33
○	27	5	-2334.95	-6.33
○	27	6	-2334.91	-6.33
○	28	0	-2334.88	-6.39
○	28	1	-2334.86	-6.39
○	28	2	-2334.26	-6.15
○	28	3	-2334.24	-6.15
○	28	4	-2334.22	-6.16
○	28	5	-2333.40	-6.18
○	28	6	-2333.36	-6.19

Show	Cluster	Element	FullFitness (kcal/mol)	Estimated ΔG (kcal/mol)
◯	28	7	-2333.35	-6.18
◯	29	0	-2334.86	-6.63
◯	29	1	-2334.83	-6.62
◯	29	2	-2334.83	-6.63
◯	29	3	-2334.79	-6.45
◯	29	4	-2334.77	-6.44
◯	29	5	-2334.75	-6.45
◯	29	6	-2331.66	-6.20
◯	29	7	-2330.79	-6.11
◯	30	0	-2334.06	-6.23
◯	31	0	-2333.81	-6.39
◯	31	1	-2333.76	-6.38
◯	31	2	-2332.85	-6.31
◯	31	3	-2332.84	-6.31
◯	32	0	-2333.34	-6.40
◯	33	0	-2333.33	-6.31
◯	33	1	-2332.64	-6.31
◯	34	0	-2333.12	-6.25
◯	34	1	-2331.68	-6.26
◯	34	2	-2331.66	-6.26
◯	35	0	-2332.64	-6.42
◯	36	0	-2331.35	-6.19
◯	37	0	-2327.22	-6.08
◯	37	0	-2327.22	-6.08